IEEE Access
Multidisciplinary | Rapid Review | Open Access Journal

Received September 8, 2021, accepted October 5, 2021, date of publication October 18, 2021,
date of current version December 21, 2021.

Digital Object Identifier 10.1109/ACCESS.2021.3121139

Branch Analysis of Macro-Traffic Flow Model With Different Driving Characteristics in Its Environment

WENHUAN AI[1], TAO XING[1], YUHANG SU[1], AND DAWEI LIU[2]
[1]College of Computer Science and Engineering, Northwest Normal University, Lanzhou, Gansu 730070, China
[2]College of Electrical Engineering, Lanzhou Institute of Technology, Lanzhou, Gansu 730050, China

Corresponding author: Wenhuan Ai (wenhuan618@163.com)

This work was supported in part by the National Natural Science Foundation of China under Grant 61863032 and Grant 11965019, in part by the China Postdoctoral Science Foundation Funded Project under Project 2018M633653XB, and in part by the "Qizhi" Personnel Training Support Project of Lanzhou Institute of Technology under Grant 2018QZ-11.

ABSTRACT Research of traffic phenomena is the application basis of intelligent transportation systems and plays an important role in enriching the theoretical system of modern traffic flow. Various nonlinear traffic phenomena in the transportation system often alternately change, and the essence of these changes is theoretically a branching behavior. When the traffic system parameters change to a critical value, the qualitative state of the traffic flow, such as the free-running state, the blocking state, and the stop-and-go state, will undergo abrupt changes. However, previous studies on the bifurcation phenomenon of traffic flow mainly focused on the microscopic car-following model from the perspective of local stability, and the bifurcation analysis of the macroscopic traffic flow model has not been reported. Therefore, this article applies branch theory to study the classic macroscopic traffic flow model. First, the types of equilibrium points and their stable states of the model equations are studied, and the global distribution structure of the equilibrium points in the phase plane is drawn to verify the consistency of the numerical and analytical solutions. Secondly, the theory deduces the existence conditions of the model, and simulations have obtained various systems such as Hopf bifurcation, saddle knot bifurcation, limit cycle bifurcation, cusp bifurcation (CP), Bogdanov-Takens (BT) bifurcation, and so on. Finally, starting from the Hopf branch and the saddle-node branch point, by drawing the density space-time diagram of the system, the stop-and-go phenomenon and local aggregation phenomenon in actual traffic are better explained. The results obtained in this paper show that the branch analysis method can better describe the nonlinear traffic phenomena on urban roads, and can provide a theoretical basis for the implementation of traffic control strategies. At the same time, it also has a very broad application prospect for the development of traffic control software in intelligent transportation systems.

INDEX TERMS Intelligent transportation system, computer simulation, nonlinear traffic phenomenon, stability analysis, branch analysis, traffic congestion.

I. INTRODUCTION

In today's rapid economic development, building a strong transportation country is an important support for comprehensively building a modern and powerful socialist country. However, as traffic demand continues to increase, the number of motor vehicles continues to increase, which intensifies the degree of congestion in the city and reduces travel efficiency. To solve the problem of traffic congestion, we cannot simply increase the number of traffic roads and restrict vehicles. We must rely on theoretical analysis and research of traffic flow, deeply think about the internal mechanism of traffic phenomena, dredge and control traffic, and alleviate and prevent traffic congestion.

Intelligent Transportation Systems (ITS) is currently the international public as one of the effective measures to solve the problem of urban traffic congestion. The system relies on real-time traffic flow to deliver the hand way, the effective analysis and control of the traffic system, to achieve the maximum alleviation of traffic congestion. The study of traffic

The associate editor coordinating the review of this manuscript and approving it for publication was Amjad Mehmood.

phenomena is the basis of applications in the fields of intelligent transportation systems, plays an important role in enriching the theoretical system of modern traffic flow. Researchers analyze actual traffic phenomena and use traffic flow theory to establish a mathematical model that can describe the general characteristics of the traffic, explore the relationship between traffic flow density and speed, reproduce complex traffic phenomena. The mathematical model describing the actual traffic law is the main tool to reveal the basic law of traffic flow. Researchers have now proposed a large number of traffic flow models, mainly including three types: cellular automata model [1]–[3], micro car-following model [4]–[8], and macro dynamics model [9]–[13]. However, due to the complexity of the traffic system, various traffic phenomena in actual traffic such as stop-and-walk phenomenon, increased vehicle density, increased vehicle speed, etc. often appear alternately, and it is difficult to find a universal model to solve all problems. Secondly, since the previous research on traffic flow theory mainly focused on the microscopic car-following model, the study of traffic flow phenomena from the perspective of local stability has limitations. The new generation of intelligent transportation systems puts forward a higher level of research on traffic phenomena. The research on the microscopic car-following model traffic flow phenomenon can no longer meet the needs of current intelligent systems. Therefore, this paper proposes a branch analysis method of a macroscopic traffic model, which can describe and predict the nonlinear traffic phenomena on the road from the perspective of the global stability of the system. The study of traffic flow branching theory can not only effectively explain various traffic flow phenomena, but also contribute to the development of traffic control software in intelligent transportation systems.

The transportation system is a complex integrated system and a time-varying nonlinear dynamic system. There are complex non-linear relationships among the various factors that make up the transportation system, and the various factors that reflect traffic characteristics and affect traffic are also non-linear, which makes a large number of nonlinear phenomena in the transportation system. At present, researchers have further analyzed traffic system problems from the perspective of nonlinear scientific theory. For example, in 2001, Y. Igarashi *et al.* proved that there will be multiple exact solutions in a certain range of automobile density in the optimal speed model with time lag, and confirmed the existence of the subcritical Hopf branch [14]. In 2002, L.A. Safonov *et al.* studied the phenomena of Hopf branch and limit cycle caused by the delay time of the driver [15]. In the same year, H.J.C. Huijberts *et al.* studied the synchronous movement of the circular bus route following the model, found their local stability described the branches of the synchronous movement [16]. In 2004, Orosz.G *et al.* found the Hopf bifurcation point after analyzing the stability of the steady-state solution and local branching in the study of the optimal speed model of the driver's reflection time [17]. In the same year, I. Gasser described the model of N cars on a ring road and found that if the density of the cars is changed, it will prove that the loss of stability is usually caused by the Hopf branch [18]. In 2006, Liu *et al.* considered branching to be one of the main reasons for various nonlinear behaviors in traffic flow, and reviewed the current research on branching phenomena in traffic flow [19]. In 2008, Zhou Wei *et al.* analyzed the cycle-doubling bifurcation and chaos phenomena in traffic flow through a new type of traffic flow car-following model [20]. In 2009, Ling Daijian *et al.* studied a class of nonlinear time-delay car-following models, analyzed the stability of the system and Hopf branch characteristics and obtained the influence of the driver's response time and safety distance on the stability range of the system [21]. In 2010, Jin Yanfei *et al.* used the Hopf bifurcation theory to calculate the full speed difference vehicle following model using Hopf bifurcation theory. The study found that the Hopf bifurcation critical point is located at the boundary of the linearly unstable regions, the uniform traffic flow will lose linear stability and appear when passing through the Hopf bifurcation point [22]. In 2013, Xu Jian *et al.* reviewed the research on various branching phenomena in the time-delayed car-following model with continuous time and space, proposed to study various nonlinear traffic phenomena in the time-delayed car-following model through the theory of time-delay dynamic system [23]. In 2015, Delgado.J *et al.* studied the traveling wave solution of the Kerner-Konhauser model and proved the existence of the DTB branch in the model, thus explaining the existence of the Hopf branch and the GH branch in the model, and compared it with the GH branch curve, depicts the stability limit cycle of the system [24]. In 2017, Yasunari Miura *et al.*'s analysis of the optimal speed traffic flow model revealed a branch structure [25]. In 2018, in a heterogeneous traffic flow model with periodic boundary conditions, Yu-Qing *et al.* used branch analysis to discuss the branching mode of the heterogeneous system in three cases in detail, explained the branching pattern diagram [26]. In the same year, Wang Wei *et al.* obtained two balance points by solving the low-dimensional macroscopic traffic flow model, and discussed its stability, and found that the model has a transcritical bifurcation point [27]. In 2020, Ren Weilin *et al.* carried out a bifurcation analysis on the heterogeneous continuous traffic flow model that took into account the differences in the psychological travel of drivers, and discussed the existence and stability of the Hopf bifurcation from a theoretical perspective [28]. At the same time, Zhu *et al.* proposed a new short-term traffic flow prediction method based on wavelet transform (WT) and multidimensional Taylor network (MTN). The proposed prediction model provides better prediction performance and time correlation. In addition, when considering data from different dates and locations, the new model shows good robustness and generalization ability [29]. Arzoo Miglani *et al.* discussed various deep learning models used for self-driving vehicle traffic flow prediction and compared the applicability of these models in modern intelligent transportation systems [30]. Chen *et al.* used multiple heterogeneous data to establish

a random traffic flow model method based on vehicle trajectory information, revealing the internal mechanism of the complex dynamics and random evolution of traffic flow, and providing a theoretical basis for a new generation of intelligent transportation systems [31]. Jia *et al.* developed an enhanced cooperative micro-traffic model considering V2V and V2I communication, and studied how vehicle communication affects vehicle cooperative driving, especially in the case of traffic interference [32]. D. Ngoduy and others applied coupled Langevin equations to simulate complex human driver behaviors, used stochastic processes to describe time-varying random acceleration, and proposed a new continuous stochastic car-following model to study implies a theoretical significance for the design of CACC or ACC control algorithm to reduce the negative impact of human/machine delays in traffic flow [33]. In addition, D. Ngoduy *et al.* established a multi-delay car-following model and studied the boundary of the linearly unstable region formed by the Hopf bifurcation point, and found that increasing the delay of the perception space interval will expand the unstable region, thereby destroying the traffic flow stability [34].

Traffic flow bifurcation phenomenon refers to the phenomenon that when the system parameters change and exceed a certain critical value, the stable state of the traffic system changes substantially, such as the transition between the free-running state, walking stop state, traffic congestion, and other traffic states. To deal with traffic congestion, the nonlinear dynamic behavior of traffic flow at the branch critical point should be well understood by people. At present, branch as the main concept of nonlinear scientific theory has attracted wide attention of researchers. It starts from the most common traffic flow state instability phenomenon in traffic flow and explores the internal state changes hidden in the complex traffic flow system. The mechanism provides a new method to reveal the inherent regularity behind the phenomenon of nonlinear traffic flow, to detect and relieve traffic congestion in time. However, the researchers mainly study the phenomenon of traffic flow branching based on the car-following model. Compared with the car-following model, the macro-traffic flow model can better describe the collective behavior of traffic flow and is more suitable for dealing with traffic flow problems composed of a large number of vehicles, to relieve and prevent traffic congestion. At present, there are few studies on the analysis of traffic flow branching phenomena based on the macroscopic traffic flow model. Therefore, the traffic flow real-time transmission system in the ITS system is used to carry out statistical analysis on the density and average speed of the actual traffic flow, which provides data support for the study of traffic flow branching phenomena. Using the branch analysis method, the nonlinear dynamic behavior of traffic flow at various branch points in the system is analyzed through the density space-time diagram and the branch phase plane diagram. According to unstable branch points, specific management control strategies under different situations are proposed. Use traffic information boards, traffic guidance variable display screens, etc. to adjust traffic flow, density, and other data, thereby changing the appearance or nature of branch points, turning unstable branch points into stable branch points or disappearing, and at the same time, feedback the analysis results to ITS system realizes congestion mitigation or preventive control.

The remainder of the paper is organized as follows. In Section 2, a new macroscopic traffic flow model is proposed through variable substitution. In Section 3, the classification and stability of the equilibrium points of the new model are studied and the overall distribution structure of the nearby equilibrium solutions are drew in the phase plane by selecting four sets of parameters. In Section 4, the existence conditions of Hopf bifurcation and saddle-node bifurcation of the model is proved. Then various bifurcations of the system such as Hopf bifurcation, saddle-node bifurcation and Limit Point bifurcation of cycles are found by numerical simulation. In Section 5, we explained the stop-and-go wave and stability mutation in real traffic by the numerical simulations. We conclude the paper in Section 6.

II. MODEL EQUATIONS

Serge P. Hoogendoorn *et al.* proposed a macroscopic traffic flow model considering the different driving characteristics [35], which consists of the following two equations, one is the equation for the conservation of the number of vehicles,

$$\frac{\partial \rho}{\partial t} + \frac{\partial (\rho v)}{\partial x} = 0 \tag{1}$$

and an equation of motion,

$$\frac{\partial u}{\partial t} + v\frac{\partial u}{\partial x} = 2\frac{\left[V_{e(}(\rho) - v\right]}{\tau} + 2v\frac{\partial \rho}{\partial x} + \frac{k}{\rho}\frac{\partial^2 v}{\partial x^2} \tag{2}$$

where ρ is the density, v is the velocity, τ is the driver reaction time, k is the speed difference of different driving characteristics, $\frac{\partial^2 v}{\partial x^2}$ is a sticky item, its role is to help eliminate the impact or discontinuities, without significantly changing the dissection of the original model. $V_e(\rho)$ is the optimal velocity function and has the following form:

$$V_e[\rho] = \mathrm{v}_f \left\{ \left[1 + \exp\left(\frac{\rho/\rho_m - 0.25}{0.06} \right) \right]^{-1} - 3.72 \times 10^{-6} \right\} \tag{3}$$

Here $v_f = 30\mathrm{m/s}$ is the free-flow speed, $\rho_m = 0.2veh/m$ is the maximum or jam density and the related parameters of the model are set as follows: T=10s, $c_0 = 11m/s$, $\mu_0 = 550$.

Assuming that the model has a traveling wave solution $\rho(z)$ and $v(z)$, where $z = x - ct$, traveling wave velocity $c < 0$. Bring it into the equation (1) and (2), can get:

$$-c\rho_z + q_z = 0 \tag{4}$$

$$-cv_z + vv_z = \frac{2V_e - 2V_e k - 2u - uk - 2\tau k V_e \rho_z + kv_z}{\tau k} + \frac{k\delta^2}{2\tau k} v_{zz} \tag{5}$$

where q is the flow which equals the product of the density and speed. From Eq. (4), get:

$$v_z = \frac{c\rho_z}{\rho} - \frac{q\rho_z}{\rho^2} \tag{6}$$

The integration of Eq. (4) over z yields:

$$-c\rho + q = const = q_* \tag{7}$$

$$q = q_* + c\rho \tag{8}$$

Substituting Eq. (6) and (8) into Eq. (2), we obtain:

$$\rho_{zz} + \left(\frac{q_*^2\rho k - q_*^3 k - kV_e(\rho)\, q_*^2\rho^3}{\tau}\right) \times \rho_z - \frac{1}{\tau}\left(V_e(\rho) - \frac{q_*}{\rho} - k\right) = 0 \tag{9}$$

The equation may be written as the following second-order ordinary differential equation for solving $\rho(z)$:

$$\rho_{zz} - g(\rho, q_*)\,\rho_z - f(\rho, c, q_*) = 0 \tag{10}$$

where:

$$g(\rho, q_*) = \frac{kq_*^2\left[\tau c_0\rho - kq_* - kV_e(\rho)\,\rho^3\right]}{\tau} \tag{11}$$

$$f(\rho, c, q_*) = f(\rho, c, q_*) = \frac{\rho}{\tau k q_*}\left[q_* + k\rho - \rho V_e(\rho)\right] \tag{12}$$

Let $y = \frac{d\rho}{dz}$ Then, Eq. (10) is transformed as follows:

$$\begin{cases} \dfrac{d\rho}{dz} = y \\ \dfrac{d\tilde{y}}{dz} = g(\rho, q_*)\, y + f(\rho, c, q_*) \end{cases} \tag{13}$$

III. TYPES AND STABILITIES OF EQUILIBRIUM POINTS IN THE MODEL

The significance of studying the type and stability of the balance point of the new model is to find the various branch points of the transportation system from the balance point as the starting point on the phase plan and draw the global distribution structure of the traffic trajectory near the branch point. Theoretically analyze the possible branches of the traffic system, branch conditions, and the stability changes of the traffic flow passing these branch points.

If we set the terms on the right-hand side of Eq. (13) to be zero, then we have $y = 0$ and $F = 0$. So the equilibrium points $(\rho_i, 0)$ of the system can be determined. The linearized system of Eq. (13) can be derived through the Taylor expansion at the equilibrium points and we write it as follows:

$$\begin{cases} \dfrac{d\rho}{dz} = y \\ \dfrac{dy}{dz} = G(\rho_i, q_*)\, y + F'(\rho_i, c, q_*)(\rho - \rho_i) \end{cases} \tag{14}$$

The Jacobian characteristic equation of (14) reads:

$$\lambda^2 - G_i\lambda - F_i' = 0 \tag{15}$$

where $G_i = G(\rho_i, q_*)$ and $F_i' = \mathrm{F}'(\rho_i, c, q_*)$.

TABLE 1. Types and stabilities of some equilibrium points of the linearized system (14) with the given parameters, where $\Delta_i = G_i^2 + 4F_i', i = 1, 2, 3$.

	ρ_1	ρ_2	ρ_3
$(c, q_*) = (-1.371, 0.2)$	0.0065 $F_i' > 0$, saddle point, unstable for $z \to \pm\infty$	0.0937 $\Delta_i < 0$, $G_i < 0$, spiral point, stable for $z \to +\infty$, unstable for $z \to -\infty$	0.1447 $F_i' > 0$, saddle point, unstable for $z \to \pm\infty$
$(c, q_*) = (-1.38, 0.64)$	0.0226 $F_i' > 0$, saddle point, unstable for $z \to \pm\infty$	0.1269 $\Delta_i < 0$, $G_i < 0$, spiral point, stable for $z \to +\infty$, unstable for $z \to -\infty$	
$(c, q_*) = (-2.5, 0.8)$	0.0282 $F_i' > 0$, saddle point, unstable for $z \to \pm\infty$	0.0546 $\Delta_i < 0$, $G_i < 0$, spiral point, stable for $z \to +\infty$, unstable for $z \to -\infty$	
$(c, q_*) = (-6.7, 0.2)$	0.0041 $F_i' > 0$, saddle point, unstable for $z \to \pm\infty$		

According to the qualitative theory of differential equations, the types of the equilibrium point $(\rho_i, 0)$ for the system (14) can be judged as (a) a saddle point for $F_i' > 0$; (b) a nodal point for $G_i^2 + 4F_i' > 0$ with $F_i' < 0$; (c)a spiral point for $G_i^2 + 4F_i' < 0$ with $G_i \neq 0$, and (d) a center for $F_i' < 0$ and $G_i = 0$. The system is always unstable at a saddle point for $z \to \pm\infty$. It is stable at a nodal or a spiral point for $z \to +\infty$ (or $z \to -\infty$) if $G_i < 0$ (or $G_i > 0$).

The non-linear system (13) shares the same equilibrium points as the linearized system (14). Moreover, the two systems are uniformly stable or unstable at these equilibrium points if the equilibrium point is not the center point according to the Hartman-Gorban linearization theorem. The equilibrium points $\rho_i\,(i = 1, 2, \ldots)$ of the linearized system of Eq. (14) can be solved when parameter values of c and q_* are given. We can identify the types and stabilities of these points according to the discussion mentioned above. Next, we take four sets of parameter values for examples and show the results in Table 1. It is to be noted here that $\rho_i = 5$ is a trivial equilibrium point and has no practical significance because ρ is equal to 0 at this time. So there is no need to discuss it.

Since the analytical solution of the nonlinear system (13) is unlikely to be derived, the numerical solutions nearby the equilibrium points can be given in the phase-plane. We use the four sets of parameters in Table 1 respectively to study the stabilities of system (13) at these equilibrium points. The

results are shown in Figs. 1 and 4. The equilibrium points are represented by $(\rho_i, 0)$, $i = 1, 2, 3$, $\rho_1 < \rho_2 < \rho_3$.

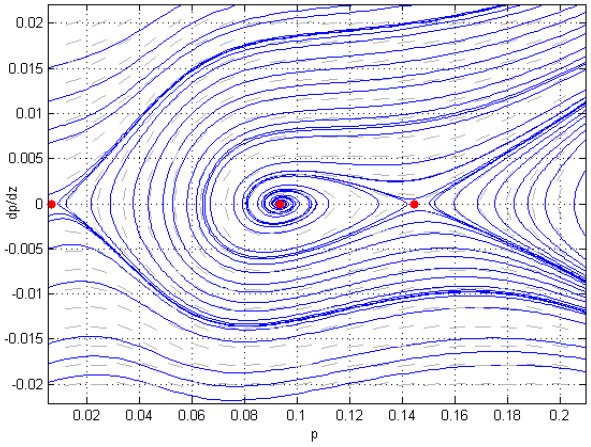

FIGURE 1. The phase plan of the trajectory corresponding to the equilibrium point when the variable parameters are $c = 1.371$ and $q_* = 0.2$.

Figure 1 corresponds to the first case in Table 1. We use the equilibrium point as the starting point to draw the trajectory distribution structure diagram of the nonlinear system, and we can find that the various equilibrium points in the phase diagram affect each other, resulting in a relationship of divergence and aggregation. From the perspective of the overall stability of the system, it shows the influence of the equilibrium point on the traffic state. This is the same as what we have observed in actual traffic. It can be seen from Figure 1: When $z \to \pm\infty$, the system is unstable at the equilibrium point $(\rho_1, 0)$ and $(\rho_3, 0)$, the trajectory close to this point is also far away from this point. When $z \to +\infty$, multiple spiral trajectories near saddle point $(\rho_3, 0)$ tend to focus $(\rho_2, 0)$. When $z \to -\infty$, these trajectories move away from the focus and eventually tend to infinity. This shows that: When $z \to +\infty$, the system is stable at $(\rho_2, 0)$; when $z \to -\infty$, the system is stable at $(\rho_2, 0)$, the trajectory can be regarded as the saddle-focus solution of the system.

Figure 2 corresponds to the second case in Table 1. As the parameters increase, we observe that the equilibrium point gradually changes from an unstable state to an aggregate state over time. This is consistent with the formation of traffic congestion in actual traffic flow over time. It can be seen from Figure 2: The system is unstable at the equilibrium point $(\rho_1, 0)$. The spiral trajectory starting from $(0.12, 0)$, when $z \to +\infty$, the spiral trajectory tends to the focus $(\rho_2, 0)$, the system is stable at this point. When $z \to -\infty$, these trajectories are far away from the focal point $(\rho_2, 0)$ and eventually form a constant amplitude oscillation, the system is unstable. Further research found that the spiral trajectory starting from $(0.06, 0)$, when $z \to -\infty$, all trajectories in the figure approach the outermost circle of the curve; when $z \to +\infty$, it tends to infinity far. Therefore, a limit cycle is created between the trajectories.

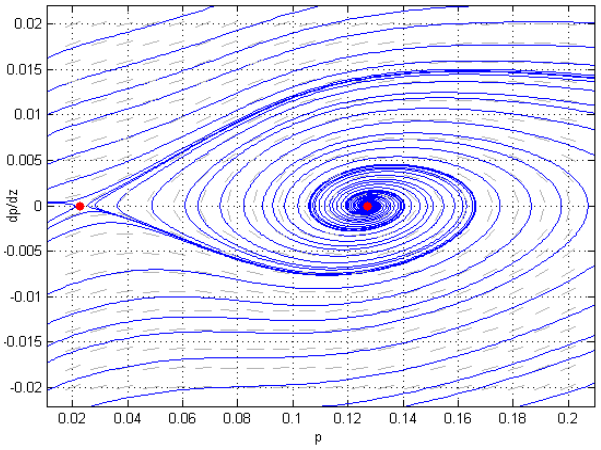

FIGURE 2. The phase plan of the trajectory corresponding to the equilibrium point when the variable parameters are $c = -1.38$ and $q_* = 0.64$.

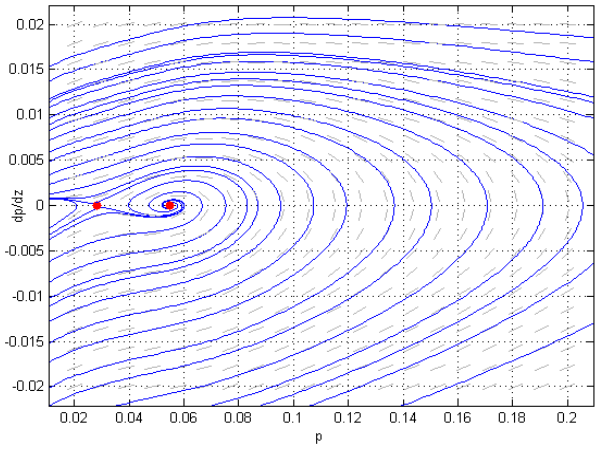

FIGURE 3. The phase plan of the trajectory corresponding to the equilibrium point when the variable parameters are $c = -2.5$ and $q_* = 0.8$.

Figure 3 corresponds to the third case in Table 1. With the continuous increase of the parameters, we observe that the equilibrium point changes with time, and the aggregation state of the trajectory also increases significantly, which indicates that the traffic congestion has also reached the maximum. In actual traffic, the vehicle has fallen into a standstill. It can be seen from Figure 3: When $z \to \pm\infty$, the system is unstable at the equilibrium point $(\rho_1, 0)$, its nearby trajectories are far away from this point. When $z \to +\infty$, the spiral trajectory near the saddle point $(\rho_1, 0)$ tends to the focus $(\rho_2, 0)$. When $z \to -\infty$, these trajectories are far away from the focal point and eventually tend to infinity. It shows that: when $z \to +\infty$, the system is stable at $(\rho_2, 0)$; when $z \to -\infty$, the system is unstable at $(\rho_2, 0)$. The spiral degree of these trajectories is obviously increased compared to Fig. 1, which is due to the absence of the function of saddle point $(\rho_3, 0)$ in Fig. 1. Because the vehicle density presents a monotonously increasing relationship, compared with Fig. 1, the vehicle density value near the focal point $(\rho_2, 0)$ also presents a larger oscillation state.

Figure 4 corresponds to the fourth case in Table 1. It can be seen from Figure 4: when $z \to \pm\infty$, the system is unstable at the equilibrium point $(\rho_1, 0)$, its nearby trajectories are far away from this point. Since the value of vehicle density in the figure continues to show a monotonous increasing relationship, it indicates that the value of vehicle density corresponding to this set of parameters will also continue to increase, and the transportation system is unstable and eventually tends to be congested.

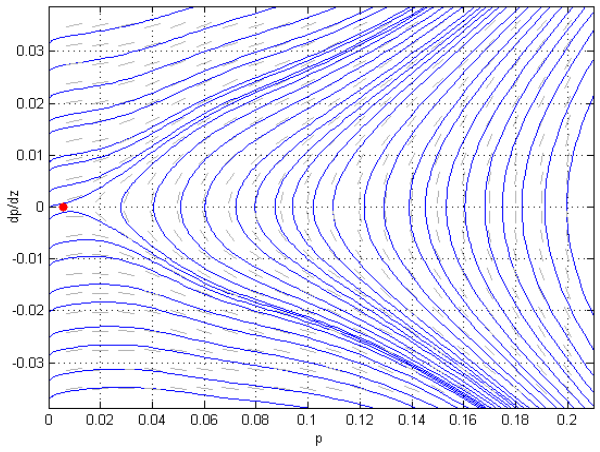

FIGURE 4. The phase plan of the trajectory corresponding to the equilibrium point when the variable parameters are $c = -6.7$ and $q_* = 0.2$.

It can be seen from the above figure that the type and stability of the equilibrium point on the phase plane are consistent with the theoretical results in Table 1. In addition, they show the influence of the equilibrium point on the traffic state from the perspective of the global stability of the system.

IV. BIFURCATION ANALYSES

A. HOPF BIFURCATION CONDITIONAL DERIVATION

According to the Hopf bifurcation condition theorem given in literature [36], analysis of system (13), let q_* be a variable parameter, which has an equilibrium point $(\rho_0, 0)$ for all q_*. The derivative matrix L at the equilibrium point is also the Jacobian matrix of the system at the equilibrium point, as follows in (16), as shown at the bottom of the page.

Because the equilibrium point satisfies equations $y = 0$ and $F = 0$, we have $q_*\rho + (1 - \rho_m\rho)(V_e(\rho) - c) = 0$ and the Eq. (14) can be rewrite as (17), shown at the bottom of the page.

Let its eigenvalue be $\lambda, \lambda = \alpha(q_*) \pm i\beta(q_*)$, then its characteristic equation is:

$$\lambda^2 - (A_1 + A_4)\lambda + (A_1A_4 - A_2A_3) = 0 \tag{18}$$

Suppose that the equation has a pair of complex eigenvalues $\alpha(q_*) \pm i\beta(q_*)$, then (19)–(21), as shown at the bottom of the page.

Since $V_*'(\rho) < 0$, c is not equal to 0. Let $\alpha(\rho_0, q_{*_0}) = 0$, get:

$$\alpha\left(\rho_0, q_{*_0}\right) = \frac{\rho^2 q_*^2 + k^2(\rho_m\rho - 1)^2}{2\tau^2(\rho_m\rho - 1)\rho q_*^2}\Big|_{q_* = q_{*_0}} \triangleq 0 \tag{22}$$

$$\Rightarrow q_{*_0} = \frac{k(\rho_m\rho_0 - 1)}{\rho_0} \tag{23}$$

$$L(q_*) = \left(\begin{array}{cc} 0 & 1 \\ \frac{-2y^2}{\rho^2} - \frac{y}{k}\left(\frac{q_*}{(\rho_m\rho - 1)^2} + \frac{k^2}{q_*\rho^2}\right) + \frac{1 - 2\rho_m\rho}{\tau} + \frac{(1 - \rho_m\rho)^2 V_e'(\rho) + 2\rho_m(\rho_m\rho - 1)(V_e(\rho) - c)}{\tau q_*} & \frac{4y}{\rho} + \frac{1}{\tau}\left(\frac{q_*\rho}{\rho_m\rho - 1} - k\right) \end{array} \right)\Bigg|_{\substack{\eta = \eta_0 \\ y = y_0 \\ q_* = q_{*_0}}} \tag{16}$$

$$L(q_*) = \left(\begin{array}{cc} 0 & 1 \\ \frac{q_* + (1 - \rho_m\rho)^2 V_e'(\rho)}{\tau k}\frac{1}{\tau^2} & \left(\frac{q_*\rho}{\rho_m\rho - 1} - \frac{\gamma^2(\rho_m\rho - 1)}{q_*\rho}\right) \end{array} \right)\Bigg|_{\substack{\eta = \eta_0 \\ y = y_0 \\ q_* = q_{*_0}}} \triangleq \begin{pmatrix} A_1 & A_2 \\ A_3 & A_4 \end{pmatrix} \tag{17}$$

$$\alpha(q_*) = \frac{A_1 + A_4}{2} = \frac{1}{2\tau^2}\left(\frac{q_*\rho}{\rho_m\rho - 1} - \frac{k^2(\rho_m\rho - 1)}{q_*\rho}\right) \tag{19}$$

$$\begin{aligned} \beta(q_*) &= \sqrt{(A_1A_4 - A_2A_3) - \frac{(A_1 + A_4)^2}{4}} \\ &= \sqrt{-\frac{1}{4\tau^2}\left(\frac{q_*\rho}{\rho_m\rho - 1} - \frac{k^2(\rho_m\rho - 1)}{q_*\rho}\right)^2 - \frac{q_* + (1 - \rho_m\rho)^2 V_e'(\rho)}{\tau k}} \end{aligned} \tag{20}$$

$$c = \dot{a}(q_*)|_{q_{*_0}} = \frac{\rho}{2\tau^2(\rho_m\rho - 1)} + \frac{k^2(\rho_m\rho - 1)}{2\tau^2 q_*^2\rho} = \frac{\rho^2 q_*^2 + k^2(\rho_m\rho - 1)^2}{2\tau^2(\rho_m\rho - 1)\rho q_*^2} \neq 0 \tag{21}$$

So we have:

$$\beta\left(\rho_0, q_{*_0}\right) = \sqrt{\frac{-q_* - (1-\rho_m\rho)^2 V_e'(\rho)}{\tau k q_*}}\Bigg|_{\substack{\eta=\eta_0 \\ q_*=q_{*_0}}} \tag{24}$$

Because of $V_*'(\rho) < 0$, when $-\rho_0^2 V_*'(\rho_0) > q_{*_0} > 0$, $\beta(\rho_0, q_{*_0}) > 0$. At this time, the system has Hopf bifurcation at $q_* = q_{*_0}$.

B. THE HOPF TYPE DERIVATION OF THE MODEL

For the Hopf bifurcation problem, because the ndimensi-onal system can be restricted to the 2-dimensional center manifold by the center manifold method, only the Hopf bifurcation of the 2-dimensional system is considered.

Lemma 3.1 ([36]): suppose a two-dimensional system with parameters

$$x' = f(x, \gamma)\, x = (x_1, x_2)^T \in R^2, \quad \gamma \in R \tag{25}$$

The equilibrium point is the origin $O(0, 0)$, and the eigenvalue at the origin is $\alpha(\gamma) \pm i\omega(\gamma)$. And when $\gamma = 0$, the partial derivative matrix of the system has pure imaginary eigenvalue $i\omega_0$, that is $\alpha(0) = 0, \omega(0) = \omega_0 > 0$. Through coordinate transformation, the system (25) can be written as:

$$\begin{cases} x_1' = \alpha(\gamma)\, x_1 - \omega(\gamma)\, x_2 + \tilde{f}_1(x_1, x_2, \gamma) \\ x_2' = \omega(\gamma)\, x_1 + \alpha(\gamma)\, x_2 + \tilde{f}_2(x_1, x_2, \gamma) \end{cases} \tag{26}$$

where $\tilde{f}_1, \tilde{f}_2 = O\left(x_1^2 + x_2^2\right)$∘

Theorem 4.1: (Hopf bifurcation theorem of ODE) suppose that the partial derivative matrix $D(\gamma)$ of the system (25) at the origin has an eigenvalue $\alpha(\gamma) \pm i\omega(\gamma)$ and satisfies $\alpha(0) = 0, \omega(0) = \omega_0 > 0$ and $c = \alpha'(0) \neq 0$, then there exists an analytic function.

$$\gamma(\varepsilon) = \sum_{k=2}^{\infty} \gamma_k \varepsilon^k \tag{27}$$

So that for $\gamma = \gamma(\varepsilon) \neq 0$, the system (26) has a unique closed orbit Γ_ε in a sufficiently small neighborhood of the origin, and its period:

$$T(\varepsilon) = \frac{2\pi}{\omega_0}\left(1 + \sum_{k=2}^{\infty} \tau_k \varepsilon^k\right) \tag{28}$$

When $\varepsilon \to 0, \gamma(\varepsilon) \to 0, \Gamma_\varepsilon$ tend to the origin. Let γ_{k1} be the coefficient of the first term not equal to zero in the expansion (29), then when γ_{k1} and c are the same sign, Γ_ε is a stable limit cycle; when γ_{k1} and c are different sign, Γ_ε is an unstable limit cycle.

The proof of theorem 4.1 and the formula of coefficient γ_k, τ_k are given in document [44], especially when $k = 2$,

$$\gamma_2 = -a/c, \quad \tau_2 = -\left(b + \gamma_2\omega'(0)\right)/\omega_0 \tag{29}$$

Among

$$\begin{aligned} a = {} & (1/16)\left[\tilde{f}_{1xxx} + \tilde{f}_{1xyy} + \tilde{f}_{2xxy} + \tilde{f}_{2yyy}\right] + (1/16\omega_0) \\ & \times \left[\tilde{f}_{1xy}\left(\tilde{f}_{1xx} + \tilde{f}_{1yy}\right) - \tilde{f}_{2xy}\left(\tilde{f}_{2xx} + \tilde{f}_{2yy}\right)\right. \\ & \left. - \tilde{f}_{1xx}\tilde{f}_{2xx} + \tilde{f}_{1yy}\tilde{f}_{2yy}\right] \end{aligned} \tag{30}$$

For the system (13), let q_* be a variable parameter, which has an equilibrium point $(\rho_0, 0)$ for all q_*. Let $\tilde{\rho} = \rho - \rho_0$ carry out coordinate translation and move the equilibrium point to the origin. At this time, the system can be expressed as follows:

Where $\tilde{f}_{1xxx}, \tilde{f}_{2xxx}$, etc. are the partial derivatives of $\tilde{f}_1, \tilde{f}_2$ at $(0, 0, 0)$. Here a is an important parameter to judge the stability of limit cycle. Assuming that the condition of theorem 4.1 holds, according to the Hopf bifurcation, the following stability conclusions are obtained.

(I) If $a < 0\,(> 0)$, then the limit cycle Γ_ε is stable (unstable);

(II) if a and c are of the same sign, the Hopf bifurcation is supercritical (subcritical);

(III) if $a = 0$, then the Hopf bifurcation is degenerate.

For the system (13), let q_* be a variable parameter, which has an equilibrium point $(\rho_0, 0)$ for all q_*. Let $\tilde{\rho} = \rho - \rho_0$ carry out coordinate translation and move the equilibrium point to the origin. At this time, the system can be expressed as follows:

$$\begin{cases} \tilde{\rho}' = y \\ y' = \dfrac{q_*^2 + 2\tau k(\tilde{\rho} + \rho_0) q_* - \alpha(\tilde{\rho} + \rho_0)^2 c^2(\rho)}{2\tau^2 k^2 (\tilde{\rho} + \rho_0) q_* (\tilde{\rho} + \rho_0)} y \\ \quad - \dfrac{\alpha(\tilde{\rho} + \rho_0)\left[V_*(\tilde{\rho} + \rho_0)(\tilde{\rho} + \rho_0) - q_* - c_0(\tilde{\rho} + \rho_0)\right]}{2\tau^2 k^2 (\tilde{\rho} + \rho_0) q_*} \end{cases} \tag{31}$$

The system can be linearized by Taylor expansion at the equilibrium point $(\tilde{\rho}, y) = (0, 0)$.

$$\tilde{x}' = L(q_*)\,\tilde{x} + f \tag{32}$$

where f is a smooth vector function, its constituent element $f_{1,2}$ is the Taylor expansion of the least quadratic term of $\tilde{x}$, which can be expressed as follows in (33), shown at the bottom of the next page.

Jacobian matrix $L(q_*)$ can be expressed as follows:

$$\begin{aligned} & L(q_*) \\ & = L(q_*) \\ & = \begin{bmatrix} 0 & 1 \\ \dfrac{\alpha[q_* + \rho_0^2 V_*'(\rho_0)]}{2\tau^2 k^2(\rho_0) q_*} & \dfrac{q_*^2 + 2k(\rho_0) q_* - \alpha\rho_0^2 c^2(\rho_0)}{2\tau^2 k^2(\rho_0) q_* \rho_0} \end{bmatrix} \\ & = \begin{pmatrix} 0 & 1 \\ b(q_*) & d(q_*) \end{pmatrix} \end{aligned} \tag{34}$$

Its eigenvalue is the root of the following characteristic equation:

$$\lambda^2 - \sigma\lambda + \Delta = 0 \tag{35}$$

inside, $\sigma = \sigma(q_*) = d(q_*) = trL(q_*)$, $\Delta = \Delta(q_*) = -b(q_*) = \det L(q_*)$,

$$\lambda_{1,2}(q_*) = \frac{1}{2}\left(\sigma(q_*) \pm \sqrt{\sigma^2(q_*) - 4\Delta(q_*)}\right) \tag{36}$$

According to the Hopf bifurcation condition, it is shown that:

$$\sigma(0) = 0, \Delta(0) = \omega_0^2 > 0 \tag{37}$$

For smaller $|q_*|$ variables can be introduced:

$$\alpha(q_*) = \frac{1}{2}\sigma(q_*), \omega(q_*) = \frac{1}{2}\sqrt{4\Delta(q_*) - \sigma^2(q_*)} \tag{38}$$

Thus, the following eigenvalue expression can be obtained:

$$\lambda_1(q_*) = \lambda(q_*), \lambda_2(q_*) = \bar{\lambda}(q_*) \tag{39}$$

where,

$$\lambda(q_*) = \alpha(q_*) + i\omega(q_*), \alpha(0) = 0, \omega(0) = \omega_0 > 0 \tag{40}$$

Let $\omega_{re} + i\omega_{im}$ be the eigenvector of $L(q_*)$ corresponding to the eigenvalue $\lambda(q_*)$, there has:

$$L(\omega_{re} + i\omega_{im}) = i\omega_0(\omega_{re} + i\omega_{im}) \tag{41}$$

Considering that the real part and imaginary part of both sides of the equal sign are equal, we can get:

$$\begin{cases} L\omega_{im} = \omega_0\omega_{re} \\ L\omega_{re} = -\omega_0\omega_{im} \end{cases} \tag{42}$$

The finishing equation (42) is as follows:

$$L[\omega_{im} \quad \omega_{re}] = [\omega_{im} \quad \omega_{re}]\begin{bmatrix} 0 & -\omega_0 \\ \omega_0 & 0 \end{bmatrix} \tag{43}$$

Thus,

$$[\omega_{im} \quad \omega_{re}]^{-1} L[\omega_{im} \quad \omega_{re}] = \begin{bmatrix} 0 & -\omega_0 \\ \omega_0 & 0 \end{bmatrix} \tag{44}$$

Order,

$$\tilde{y} = [\omega_{im}\omega_{re}]^{-1}\tilde{x} \tag{45}$$

Namely,

$$\tilde{y}' = [\omega_{im}\omega_{re}]^{-1}\tilde{x}' \tag{46}$$

Substituting equation (32) into equation (46), we can get:

$$\begin{aligned} \tilde{y}' &= [\omega_{im}\omega_{re}]^{-1} L[\omega_{im}\omega_{re}]\tilde{y} + [\omega_{im}\omega_{re}]^{-1} f \\ &= \begin{bmatrix} 0 & -\omega_0 \\ \omega_0 & 0 \end{bmatrix}\tilde{y} + [\omega_{im}\omega_{re}]^{-1} f \end{aligned} \tag{47}$$

In addition, the eigenvector of $L(q_*)$ can be calculated as follows:

$$\omega_{re} + i\omega_{im} = \begin{bmatrix} 0 \\ 1 \end{bmatrix} + i\begin{bmatrix} -\frac{1}{\sqrt{-b(q_*)}} \\ 0 \end{bmatrix} \tag{48}$$

Substituting equation (33) and the values of ω_{im} and ω_{re} into equation (48), we obtain (49), as shown at the bottom of the next page.

Equation (49) has the same form as equation (26), so according to equation (38), the value in system (13) can be calculated as follows:

$$\begin{aligned} a = (1/16)\left[\tilde{f}_{2\tilde{y}_1\tilde{y}_1\tilde{y}_2} + \tilde{f}_{2\tilde{y}_2\tilde{y}_2\tilde{y}_2}\right] + (1/16\omega_0) \\ \times\left[-\tilde{f}_{2\tilde{y}_1\tilde{y}_2}\left(\tilde{f}_{2\tilde{y}_1\tilde{y}_1} + \tilde{f}_{2\tilde{y}_2\tilde{y}_2}\right)\right] \end{aligned} \tag{50}$$

Further, the value of C can be calculated as follows:

$$c = \alpha'(0) = \frac{1}{4kc^2\rho_0^2}\left(1 + \frac{\alpha\rho_0^2c^2}{q_*^2}\right) > 0 \tag{51}$$

Therefore, for the system (13), the Hopf bifurcation is supercritical when $a < 0$, and subcritical when $a > 0$.

C. DERIVATION OF SADDLE NODE BIFURCATION CONDITIONS

Lemma 3.2 ([36]): consider that system $\dot{x} = f(x, \lambda)$, $x \in R^n, \lambda \in R$, and λ are variable parameters. If (x_0, λ) satisfies the equilibrium condition $f(x, \lambda)|_{(x_0,\lambda_0)} = 0_{n\times 1}$, records $L = D_x f(x, \lambda)|_{(x_0,\lambda_0)}$, let ψ and ϕ are L left and right unit characteristic vectors, namely $\psi L = 0$ and $L\phi = 0$. When the following conditions satisfy, $\lambda = \lambda_0$ is the saddle node type of the system.

$$i)\ a = \boldsymbol{\psi} \cdot \frac{\partial}{\partial\lambda}\boldsymbol{f}(\boldsymbol{x}, \lambda)\big|_{(\boldsymbol{x}_0,\lambda_0)} \neq 0 \tag{52}$$

$$ii)\ b = \boldsymbol{\psi} \cdot \sum_{i=1}^{n} \boldsymbol{e}_i[\boldsymbol{\phi}^{\mathrm{T}} \frac{\partial^2}{\partial\boldsymbol{x}^2} f_i(\boldsymbol{x}, \lambda)\big|_{(\boldsymbol{x}_0,\lambda_0)}\boldsymbol{\phi}] \neq 0 \tag{53}$$

For the system (13), we let q_* be a variable parameter and the differential matrix at this equilibrium point is written as Eq. (17).

$$\boldsymbol{\psi L} = \mathbf{0} \Rightarrow \boldsymbol{\psi} = \left(\frac{1}{\tau}\left(\frac{k^2(\rho_m\rho - 1)}{q_*\rho} - \frac{q_*\rho}{\rho_m\rho - 1}\right)1\right) \tag{54}$$

By substituting $\boldsymbol{\psi}$ and $\boldsymbol{\phi}$ into Eq. (52) and Eq. (53), we have:

$$\begin{aligned} a &= \boldsymbol{\psi} \cdot \frac{\partial}{\partial q_*}\boldsymbol{f}(\boldsymbol{x}, q_*)\Big|_{(\boldsymbol{x}_0,q_{*0})} \\ &= \left(\frac{1}{\tau}\left(\frac{k^2(\rho_m\rho - 1)}{q_*\rho} - \frac{q_*\rho}{\rho_m\rho - 1}\right)1\right)\begin{pmatrix} 0 \\ \frac{(1-\rho_m\rho_0)\rho_0}{k\tau q_{*0}} \end{pmatrix} \\ &= \frac{(1 - \rho_m\rho_0)\rho_0}{k\tau q_{*0}} \neq 0 \end{aligned} \tag{55}$$

$$f = \begin{bmatrix} 0 \\ k_{11}\tilde{\rho}^2 + k_{22}y^2 + k_{12}\tilde{\rho}y + k_{111}\tilde{\rho}^3 + k_{222}y^3 + k_{112}\tilde{\rho}^2y + k_{122}\tilde{\rho}y^2 + O(\tilde{\rho}, y)^4 \end{bmatrix} \tag{33}$$

The equation $1-\rho_m\rho_0=0$ is tenable only when ρ is equal to 0. But it is a trivial equilibrium point and can be neglected. So we have $a \neq 0$. Eq. (56), as shown at the bottom of the page.

So the system (13) undergoes a saddle-node bifurcation at $q_* = q_{*_0}$, if $q_{*_0} = -(1-\rho_m\rho_0)^2 V_e'(\rho_0)$.

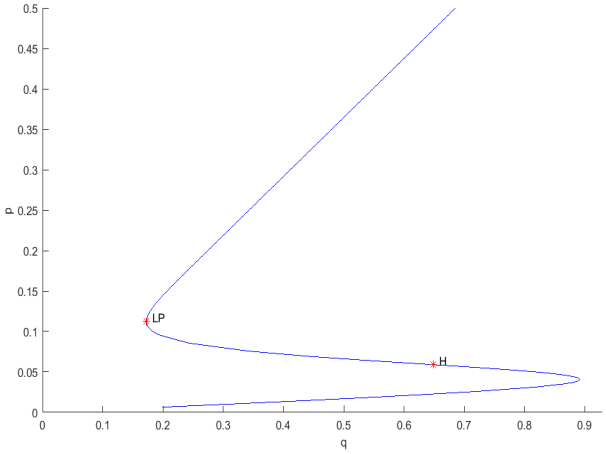

FIGURE 5. The bifurcation diagram for a wide range of the parameter q_*.

V. NUMERICAL SIMULATIONS

In order to study the various branching phenomena of nonlinear systems, we need to choose different equilibrium points as the starting point and draw the corresponding branch diagrams. Next, we use the mathematical software package MATCONT that can perform numerical analysis, select the equilibrium point $(\rho_2, 0) = (0.0546, 0)$ calculated in the third part as an example, select the parameter q_* as a variable parameter with an initial value of 0.2. The actual calculation ranges of q_* is about $-30-30$. Three special points can be found within this range. As shown in Figure 5(a), one is the Hopf branch (H) and the other is the limit point branch (LP). Figure 5(b) is a bifurcation diagram of the appropriate range of the parameter q_*.

The Hopf bifurcation point is appeared when the variable parameter q_* is taken as 0.6525412. The state variables of it are (0.0537971,0) and the corresponding vehicle density is $\rho_0 = 0.652541 veh/m$. The characteristic values of it are $-5.15597e(-8)+i0.01873044$ and $-5.15597e(-8)-i0.01873044$. That is, the real parts of the pair of conjugate eigenvalues are 0. This is considered a mark of a Hopf bifurcation.

By substituting the value of ρ_0 into the Eq. $-(1-\rho_m\rho_0)^2 V_e'(\rho_0)$, we have $-(1-\rho_m\rho_0)^2 V_e'(\rho_0) = 1.8945$. Obviously, the inequality $1.8945 > 0.64890957 > 0$ satisfies the model's Hopf bifurcation existence conditions deduced in the section 4.1. The numerical results also confirm the theory obtained.

The limit point bifurcation is appeared when the variable parameter q_* is taken as 0.19925. The state variables of it are $(0.12737, 0)$ and the corresponding vehicle density is $\rho_0 = 0.17554 veh/m$. The characteristic values of it are -0.153508 and $8.48099e-11$. That is, the second characteristic value is 0 and it is a mark of a limit point bifurcation. Moreover, the real part of the first characteristic value is negative. That means it is a stable limit point, namely a saddle-node bifurcation.

By substituting the value of ρ_0 into the Eq. $-(1-\rho_m\rho_0)^2 V_e'(\rho_0)$, we have $-(1-\rho_m\rho_0)^2 V_e'(\rho_0) = 0.1601$. Obviously, the equation $q_{*_0} = -(1-\rho_m\rho_0)^2 V_e'(\rho_0)$ satisfies

$$\begin{aligned}\tilde{y}' &= \begin{bmatrix} 0 & -\omega_0 \\ \omega_0 & 0 \end{bmatrix}\tilde{y} \\ &\quad + \begin{bmatrix} 0 \\ k_{11}\tilde{\rho}^2 + k_{22}y^2 + k_{12}\tilde{\rho}y + k_{111}\tilde{\rho}^3 + k_{222}y^3 + k_{112}\tilde{\rho}^2 y + k_{122}\tilde{\rho}y^2 + O(\tilde{\rho}, y)^4 \end{bmatrix}\end{aligned} \tag{49}$$

$$\begin{aligned} b &= \boldsymbol{\psi}\cdot\sum_{i=1}^{n} \boldsymbol{e}_i[\boldsymbol{\phi}^{\mathrm{T}}\frac{\partial^2}{\partial \boldsymbol{x}^2} f_i(\boldsymbol{x},\lambda)\big|_{(\boldsymbol{x}_0,\lambda_0)}\boldsymbol{\phi}] \\ &= \left(\frac{1}{\tau}\left(\frac{k^2(\rho_m\rho-1)}{q_*\rho} - \frac{q_*\rho}{\rho_m\rho-1}\right)\ 1\right) \\ &\quad \cdot \left(\begin{bmatrix} 1\ 0 \end{bmatrix} \begin{bmatrix} \dfrac{-2\rho_m q_* + 2\rho_m\left[\begin{array}{l}\rho_m(V_e(\rho)-k) + (1-\rho_m\rho)^2 V_e''(\rho) \\ +(\rho_m\rho-1)(1+2\rho_m)V_e'(\rho)\end{array}\right]}{k\tau q_*} - \dfrac{1}{\tau}\cdot\left[\dfrac{q_*}{(\rho_m\rho-1)^2} + \dfrac{k^2}{q_*\rho^2}\right] \\ -\dfrac{1}{\tau^2}\cdot\left[\dfrac{q_*}{(\rho_m\rho-1)^2} + \dfrac{k^2}{q_*\rho^2}\right]\dfrac{4}{\eta} \end{bmatrix} \begin{bmatrix} 1 \\ 0 \end{bmatrix} \right) \Bigg| q_* = q_{*_0} \\ &\quad [10]\begin{bmatrix} 0 & 0 \\ 0 & 0 \end{bmatrix}\begin{bmatrix} 1 \\ 0 \end{bmatrix} \\ &= \frac{-2\rho_m q_* + 2\rho_m\left[\rho_m(V_e(\rho)-k) + (\rho_m\rho-1)(1+2\rho_m)V_e'(\rho) + (1-\rho_m\rho)^2 V_e''(\rho)\right]}{k\tau q_*} \neq 0 \end{aligned} \tag{56}$$

the model's saddle-node bifurcation existence conditions deduced in the section 4.3. The numerical result is compatible with the analysis of theory.

Next, we discussed the continuation of solutions when the Hopf bifurcation point mentioned above is selected as the starting point. The first limit point bifurcation of cycles (LPC) is appeared and the parameter q_* varies to 0.64112 at this time. The period of the limit cycle is 364.61441. The corresponding bifurcation diagrams of it are shown as Fig. 6.

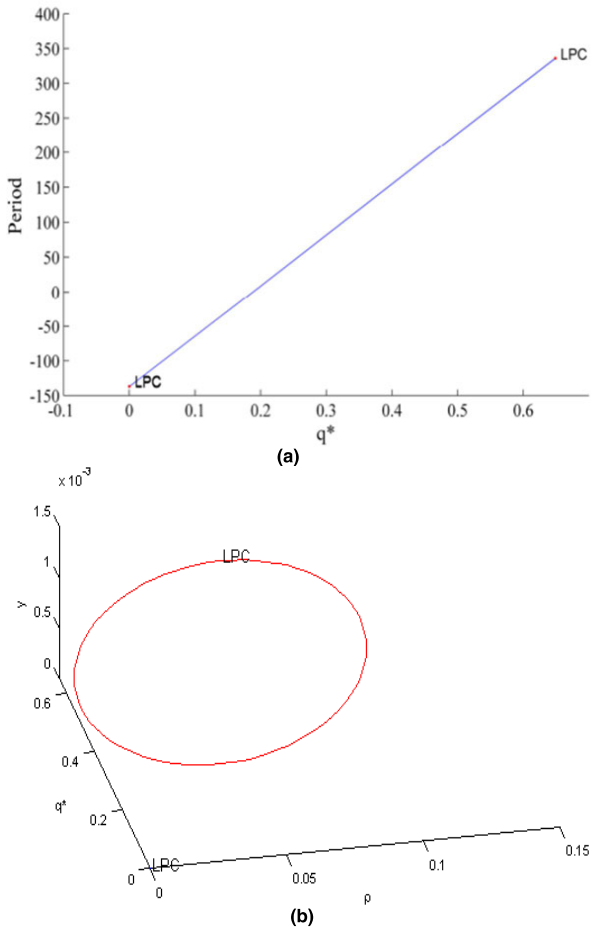

FIGURE 6. Continuation solution graph starting from Hopf branch: (a) Branch graph with variable q_* and period as coordinates; (b) Branch diagram with variables ρ, q_* and y as coordinates.

From Figure 6(a)-6(b), it can be seen that since the parameters and state variable values of the last four limit cycles are not much different, these four limit cycles almost overlap together, and compared with the first limit cycle, they are all small in size and only appear as a single point.

Next, we analyze the stability variation of traffic system when the parameters pass through some bifurcation critical points calculated above. First, to investigate the effects of Hopf bifurcation on traffic flow, we study the system stabilities in the phase-plane when q_* passes through 0.64112.

Fig.7 (a) shows that for $q_* > 0.64112$, the equilibrium point $(0.0228, 0)$ is a saddle point and the equilibrium point $(0.0589, 0)$ is a spiral point. All the curves within the red line tend to the point $(0.0589, 0)$ and this point is a sink. So the system inside the red line is stable and the system outside it is unstable.

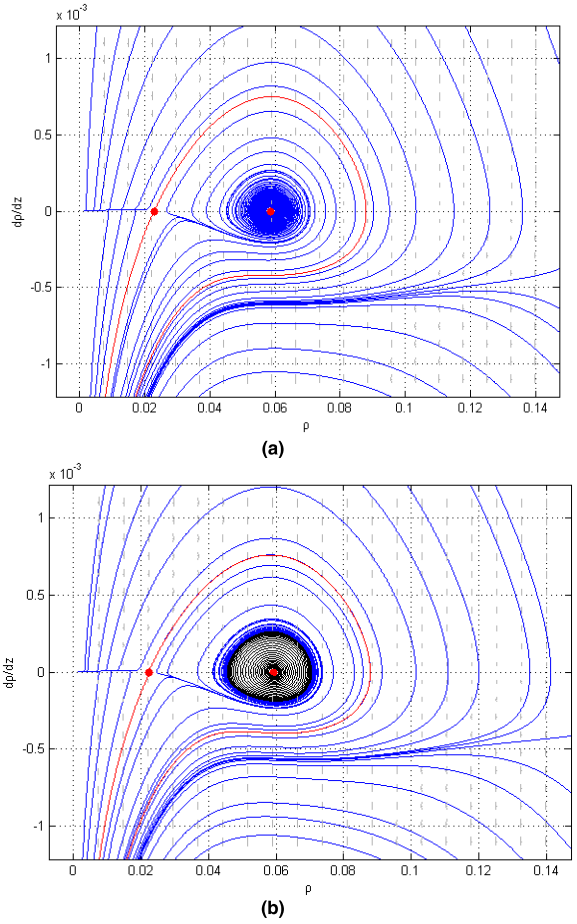

FIGURE 7. The Hopf bifurcation for $q_* > 0.64112$ and $q_* < 0.64112$: (a) Phase plane diagram when the variable parameter $q_* = 0.65$; (b) Phase plane diagram when the variable parameter $q_* = 0.638$.

It can be seen from Fig. 7(b) that for $q_* < 0.64112$, a twisted trajectory starting from $(0.05, 0)$ approaches the spiral point $(0.0593, 0)$ for $z \to +\infty$ and eventually evolves into the oscillation with the constant amplitude for $z \to -\infty$. However, a twisted trajectory goes very closely to the aforementioned area outside for $z \to -\infty$ and approaches infinity for $z \to +\infty$. So a periodic solution existed between the two trajectories. Thus no new equilibrium point arise at a Hopf bifurcation. Instead, a periodic solution is born. These theoretical analyses are also compatible with the numerical results obtained above. A limit point bifurcation of cycles (LPC) appears when q_* varies to 0.64112 and the period of it is 336.105071. Moreover, the First Lyapunov exponent $a = 6.2769562$ is greater than zero. So the Hopf bifurcation is subcritical and the limit point of cycles is unstable. The uniform traffic flow loses linear stability via Hopf bifurcation and the oscillations appear.

We can also see the effects of Hopf bifurcation in the density temporal evolution of traffic flow. By selecting the Hopf bifurcation point as the initial average density of the density temporal evolution, it may help to improve our understanding

of complex phenomena in congested traffic. The case that a localized perturbation is exerted in an initial homogeneous condition is analyzed by the traffic flow models. The initial density is used as in Ref. 21.

$$\rho(x,0) = \rho_0 + \Delta\rho_0 \left\{ \cosh^{-2}\left[\frac{160}{L}\left(x - \frac{5L}{16}\right)\right] - \frac{1}{4}\cosh^{-2}\left[\frac{40}{L}\left(x - \frac{11L}{32}\right)\right]\right\} x \in [0, L] \tag{57}$$

$$v(x,0) = V(\rho(x,0)) \quad x \in [0, L] \tag{58}$$

where ρ_0 is the initial average density, $\Delta\rho_0 = 0.01veh/m$ is the amplitude of localized perturbation, $L = 32.2km$ is the length of road section under consideration. The dynamic approximate boundary condition was given by:

$$\rho(1,t) = \rho(2,t), \quad \rho(L,t) = \rho(L-1,t), \quad v(1,t) = v(2,t), \quad v(L,t) = v(L-1,t) \tag{59}$$

For computational purpose, the space domain was divided into equal intervals of length $100m$ and time interval was chosen as $1s$. The related parameters of our model were as follows:

$$T = 10\text{s}, \quad c_0 = 11\text{m/s}, \ \mu_0 = 550, \ v_f = 30\text{m/s}, \ \rho_m = 0.2\text{veh/m} \tag{60}$$

Corresponding to the above parameters, according to the stability conditions, the critical density of the model is 0.042veh/m and 0.07veh/m, that is, the traffic flow is linearly unstable when the initial density is within the range of $0.042veh/m < \rho_0 < 0.07veh/m$.

Firstly, we select $\rho_0 = 0.058991797veh/m$ corresponding to the Hopf bifurcation point as the initial average density and the density temporal evolution is shown as the Fig.8.

From Figure 8 we can see that when the initial density value is within the unstable range of the model, as time increases, the initial small disturbance will continue to propagate downward, the amplitude of the initial small disturbance will increase with time, and finally formed a constant amplitude periodic oscillation. The traffic flow is in an unstable state.

From the nature of the Hopf branch analyzed above, it can be known that when the variable parameter passes through the Hopf branch point in the system, the transportation system will generate a limit cycle branch from the corresponding equilibrium point. This limit cycle branch can also be called a period solution. This is the characteristic of the limit cycle solution, it also illustrates the existence of the limit cycle solution.

From the results of the density space-time diagram and theoretical analysis, this is consistent with the development of an oscillating and congested traffic pattern under the uniform road conditions in actual traffic. It further shows that the obtained results are consistent with actual phenomena and numerical calculation results, which verifies the correctness of the theoretical analysis.

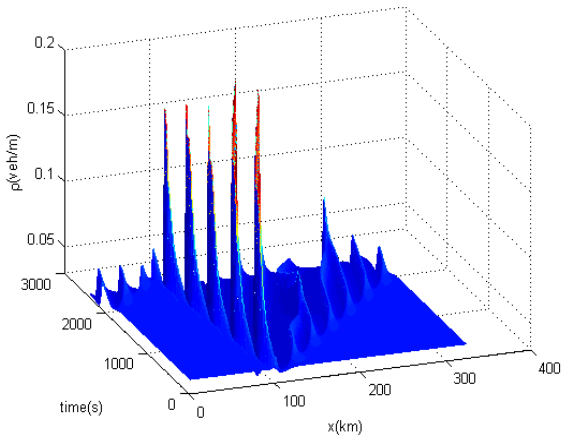

FIGURE 8. Density spatiotemporal graph with Hopf branch as initial value.

If the limit point (LP) is selected as the starting point of the bifurcation calculation, the bifurcation calculation starting at this limit point will have a bifurcation type with a codimension of 2. At the same time, the activation parameters q_* and c_1 are free parameters, and the codimension can be found to be 2 bifurcations, such as Bogdanov-Takens bifurcation (BT), cusp bifurcation (CP). The corresponding bifurcation diagram is shown in Figure 9.

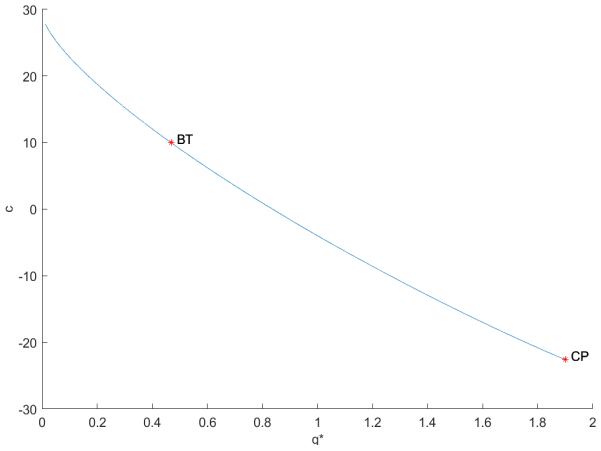

FIGURE 9. Continuation solution graph starting from the limit point branch.

BT bifurcation is obtained when the parameters $c_1 = -9.3370322, q_* = 0.92428529$, obtained the state variable of the BT bifurcation point is $(0.044025, 0)$, the two eigenvalues are $1.13868e-7+i4.43522e-5$ and $1.13868e-7-i4.43522e$, it can be considered that both eigenvalues are 0. In addition, its coefficient is $(a, b) = (4.571890e-3, -2.380277e-1)$.

CP bifurcation is obtained when the parameters $c_1 = -22.588037$, $q_* = 1.900568$, obtained the state variable of the CP bifurcation point is $(1.93756, 0)$, the two eigenvalues are $1.36395e-8$ and 0.0374581, it can be considered that both eigenvalues are 0.

Next, we study the effects of the limit point bifurcation on traffic flow when q_* passes through 0.143582.

When $q_* > 0.143582$, here we set $q_* = 0.15$. Then we have a saddle at (0.1266,0), a focus at $(0.1017, 0)$, as shown in Fig. 9(a). As the density of vehicles has been increasing monotonically, all the curves on the left of the red line are attracted and approach the point $(0.1017, 0)$. Therefore, the system on the left of the red line is stable, and the system on the right of the red line is unstable. With the change of the variable parameter q_*, the two equilibrium points gradually move closer to the middle, but when the parameter $q_* = 0.143582$, the two equilibrium points $(0.1017, 0)$ and (0.1266,0) shown in Figure10(a) merge into point $(0.1124, 0)$ One point, a saddle knot branch occurred, as shown in Figure 10(b). Similarly, the traffic system within the red line is stable, and the traffic system outside the red line is unstable. However, the curves within the red line all approach the point $(0.1124, 0)$. At this time, the linear system has a zero eigenvalue. When the variable parameters continue to change, when $q_* > 0.143582$, the equilibrium point disappears and all the solutions move to the right, as shown in Figure 10(c), the traffic system becomes unstable.

We can also see the effects of LP bifurcation in the density temporal evolution of traffic flow. By selecting the LP bifurcation point as the initial average density of the density temporal evolution, it may help to improve our understanding of complex phenomena in congested traffic. The case that a localized perturbation is exerted in an initial homogeneous condition is analyzed by the traffic flow models. The initial density is used as in Ref. 21.

$$\rho(x,0) = \rho_0 + \Delta\rho_0 \left\{ \cosh^{-2}\left[\frac{160}{L}\left(x - \frac{5L}{16}\right)\right] - \frac{1}{4}\cosh^{-2}\left[\frac{40}{L}\left(x - \frac{11L}{32}\right)\right]\right\} x \in [0, L] \tag{61}$$

$$v(x,0) = V(\rho(x,0)) \quad x \in [0, L] \tag{62}$$

where ρ_0 is the initial average density, $\Delta\rho_0 = 0.01 veh/m$ is the amplitude of localized perturbation, $L = 32.2 km$ is the length of road section under consideration. The dynamic approximate boundary condition was given by:

$$\rho(1,t) = \rho(2,t), \quad \rho(L,t) = \rho(L-1,t), \quad v(1,t) = v(2,t), \quad v(L,t) = v(L-1,t) \tag{63}$$

For computational purpose, the space domain was divided into equal intervals of length $100m$ and time interval was chosen as $1s$. The related parameters of our model were as follows:

$$T = 10\text{s}, \quad c_0 = 11\text{m/s}, \ \mu_0 = 550, \ v_f = 30\text{m/s}, \ \rho_m = 0.2\text{veh/m} \tag{64}$$

Corresponding to the above parameters, according to the stability conditions, the critical density of the model is 0.042veh/m and 0.07veh/m, that is, the traffic flow is linearly unstable when the initial density is within the range of $0.042 veh/m < \rho_0 < 0.07 veh/m$.

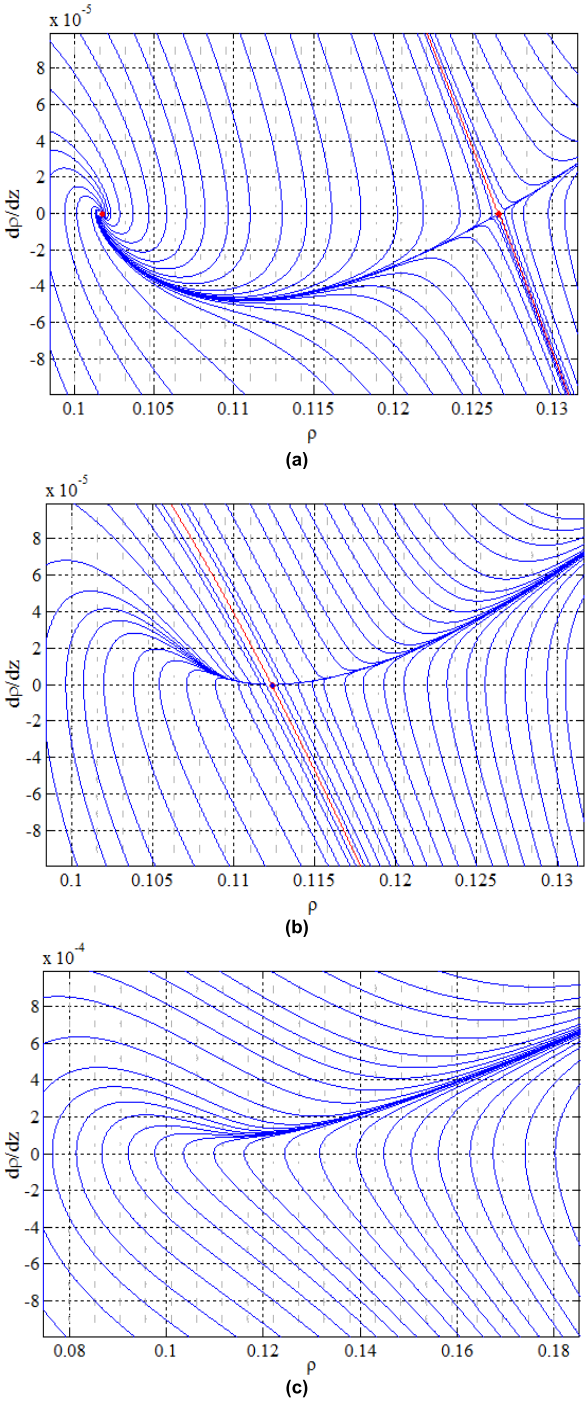

FIGURE 10. The saddle–node bifurcation when, from left to right, $q_* > 0.143582$, $q_* = 0.143582$ and $q_* < 0.143582$: (a) $q_* = 0.15$; (b) $q_* = 0.143582$; (c) $q_* = 0.13$.

Firstly, we select $\rho_0 = 0.143582 veh/m$ corresponding to the LP bifurcation point as the initial average density and the density temporal evolution is shown as the Figure 10(a)-10(b).

Knowing the nature of the LP branch, when the variable parameters pass through the LP branch point, the traffic system will produce a local clustering phenomenon from the equilibrium point. Since the initial density value at this

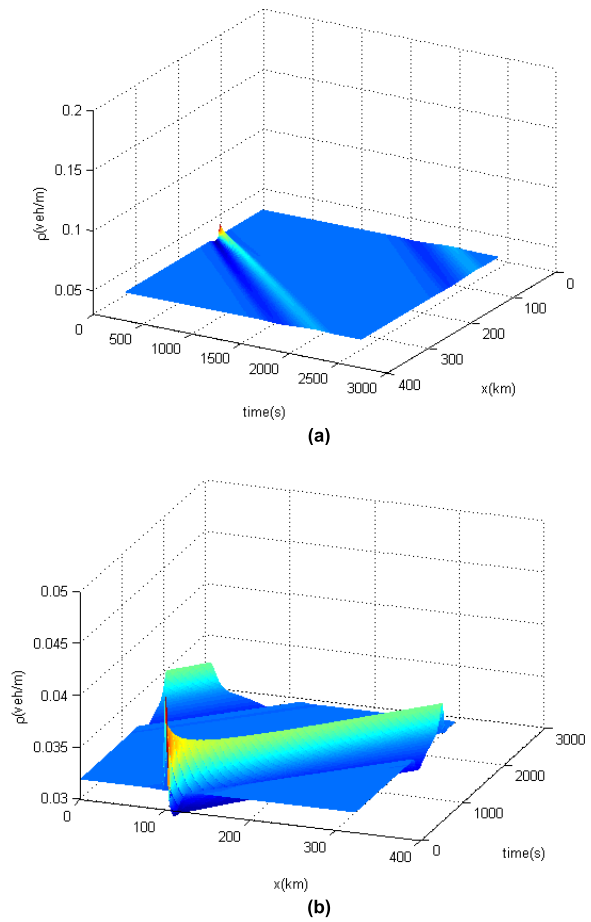

FIGURE 11. Density spatiotemporal graph with LP branch as initial value: (a) Phase plane diagram when the initial density $\rho_0 < 0.143582$veh/m; (b) Phase plane diagram when the initial density $\rho_0 > 0.143582$veh/m.

time is set within the stable range of the model, although the small disturbance on the initial uniform density is magnified, as time increases, the small disturbance eventually diverges, as shown in Figure 11(a). It can be seen from Figure 11(b) that the initial density value at this time is within the unstable range of the model, and the small disturbance on the initial uniform density is amplified, and then it evolves into a local clustering phenomenon, that is, traffic congestion. This is consistent with the characteristics of the LP branch point, which shows that under the initial uniform traffic conditions, when the parameters pass the LP branch point, the small disturbance will change into a local cluster wave, which further shows the obtained results and actual phenomena and numerical calculation results They are consistent, verifying the correctness of the theoretical analysis.

When we do not change the value of other parameters, reduce the value of v_f, choose $v_f = 20\text{m}/s$, which means that the vehicles on the road are moving forward at a moderate speed. We can see from Figure 12, The Hopf bifurcation point is appeared when the variable parameter q_* is taken as 0.5723621. The state variables of it are $(0.0497789, 0)$ and the corresponding vehicle density is $\rho_0 = 0.05723veh/m$. The characteristic values of it

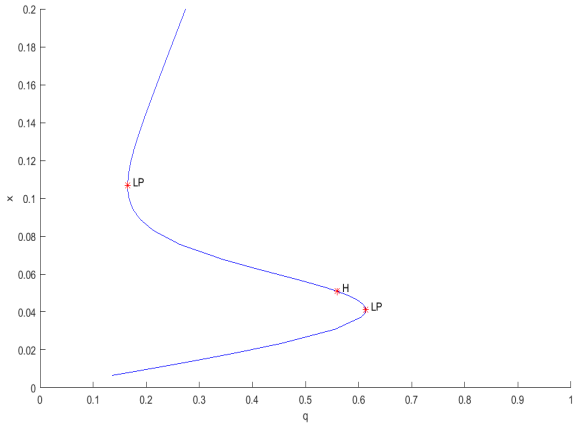

FIGURE 12. The bifurcation diagram for a wide range of the parameter q_*, $v_f = 20\text{m}/s$.

are $-5.15597e(-8) + i0.0187304$ and $-5.15597e(-8) - i0.0187304$. That is, the real parts of the pair of conjugate eigenvalues are 0. This is considered a mark of a Hopf bifurcation.

By substituting the value of ρ_0 into the Eq. $-(1-\rho_m\rho_0)^2 V_e'(\rho_0)$, we have $-(1-\rho_m\rho_0)^2 V_e'(\rho_0) = 1.8945$. Obviously, the inequality $1.8945 > 0.5723261 > 0$ satisfies the model's Hopf bifurcation existence conditions deduced in the section 4.1. The numerical results also confirm the theory obtained.

The first limit point bifurcation is appeared when the variable parameter q_* is taken as 0.61005. The state variables of it are $(0.041725, 0)$ and the corresponding vehicle density is $\rho_0 = 0.61354veh/m$. The characteristic values of it are -0.153508 and $8.48099e-11$. That is, the second characteristic value is 0 and it is a mark of a limit point bifurcation. Moreover, the real part of the first characteristic value is negative. That means it is a stable limit point, namely a saddle-node bifurcation.

By substituting the value of ρ_0 into the Eq. $-(1-\rho_m\rho_0)^2 V_e'(\rho_0)$, we have $-(1-\rho_m\rho_0)^2 V_e'(\rho_0) = 0.1601$. Obviously, the equation $q_{*_0} = -(1-\rho_m\rho_0)^2 V_e'(\rho_0)$ satisfies the model's saddle-node bifurcation existence conditions deduced in the section 4.3. The numerical result is compatible with the analysis of theory.

The second limit point bifurcation is appeared when the variable parameter q_* is taken as 0.187918. The state variables of it are $(0.113602, 0)$ and the corresponding vehicle density is $\rho_0 = 0.1806veh/m$. The characteristic values of it are $3.69898e-9$ and 0.0296604. That is, the first characteristic value is 0 and it is a mark of a limit point bifurcation.

By substituting the value of ρ_0 into the Eq. $-(1-\rho_m\rho_0)^2 V_e'(\rho_0)$, we get $-(1-\rho_m\rho_0)^2 V_e'(\rho_0) = 0.8872$. Obviously, the equation $q_{*_0} = -(1-\rho_m\rho_0)^2 V_e'(\rho_0)$ satisfies the model's saddle-node bifurcation existence conditions deduced in the section 4.3. The numerical result is compatible with the analysis of theory.

We still choose the above equilibrium point $(\rho_2, 0) = (0.0546, 0)$, and analyze the effect of the Hopf bifurcation

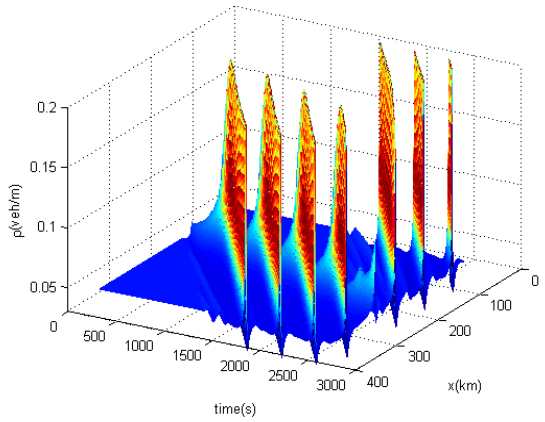

FIGURE 13. Density spatiotemporal graph with Hopf branch as initial value.

in the time evolution of traffic density when $q_* = 0.2$ and $v_f = 20$m/s. By choosing the Hopf bifurcation point as the initial average density of the density time evolution, it may help to improve our understanding of complex phenomena in congested traffic. The traffic flow model analyzes the local disturbance under the initial uniform condition. Selecting the same numerical simulation conditions as above, at this time we choose $\rho_0 = 0.057236$veh/m corresponding to the Hopf bifurcation point as the initial average density, and the time evolution of the density is shown in Figure 13.

It can be seen from Figure 13 that when the initial density value is within the instability range of the model, as time increases, the initial small disturbance will continue to propagate downward, and the amplitude of the initial small disturbance will increase with time, eventually forming a denser Large-scale periodic oscillation. The traffic flow is in an unstable state. This is a clear comparison with Figure 8.

As the vehicle speed decreases, the traffic density value gradually increases, the number of vehicles on the road section increases, the distance between vehicles becomes smaller, and the transportation system becomes unstable. Combining the density space-time diagram and the branch diagram, it can be seen that when the variable parameter q_* passes through the Hopf branch point in the system, the transportation system produces a periodic solution from the equilibrium point. The small disturbance in the initial uniform density was amplified and then evolved into a constant amplitude periodic oscillation. Small disturbance changes to stop the wave while walking. It further shows that the obtained results are consistent with actual phenomena and numerical simulation results.

We still choose the above equilibrium point $(\rho_2, 0) = (0.0546, 0)$, and analyze the effect of the LP bifurcation in the time evolution of traffic density when $q_* = 0.2$ and $v_f = 20m/s$. By choosing the LP bifurcation point as the initial average density of the density time evolution, it may help to improve our understanding of complex phenomena in congested traffic. The traffic flow model analyzes the local disturbance under the initial uniform condition. Selecting the

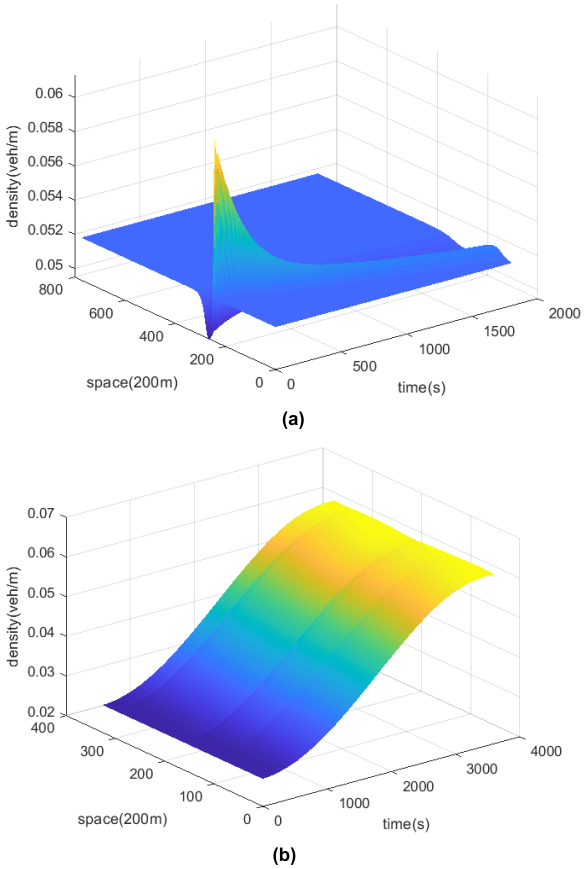

FIGURE 14. Density spatiotemporal graph with LP branch as initial value: (a) Phase plane diagram when the initial density $\rho_0 < 0.61354veh/m$; (b) Phase plane diagram when the initial density $\rho_0 > 0.61354veh/m$.

same numerical simulation conditions as above, at this time we choose $\rho_0 = 0.61354$veh/m corresponding to the LP bifurcation point as the initial average density, and the time evolution of the density is shown in Figure 14.

We can see from the above-mentioned density space-time diagram that the traffic system will produce a local clustering phenomenon from the equilibrium point. The transportation system will generate local clustering from the equilibrium point. Compared with Fig. 11(a), with the increase of time, the small disturbance is greatly amplified, but eventually diverges, as shown in Fig. 14(a). It can be seen from Figure 14(b) that the small disturbance of the initial uniform density is greatly amplified and then evolved into a strong local clustering phenomenon, that is, severe traffic congestion, which has a significant change from Figure 11(b). This shows that the decrease in vehicle speed, the sharp increase in traffic volume, the smaller the distance between vehicles, and the rapid traffic congestion. This is in obvious contrast with Figure 11.

When do not change the value of other parameters, continue to reduce the value of v_f, choose $v_f = 15$, which means that the vehicles on the road are moving forward at a low speed. We can see from Figure 15, the Hopf bifurcation point is appeared when the variable parameter q_* is taken as

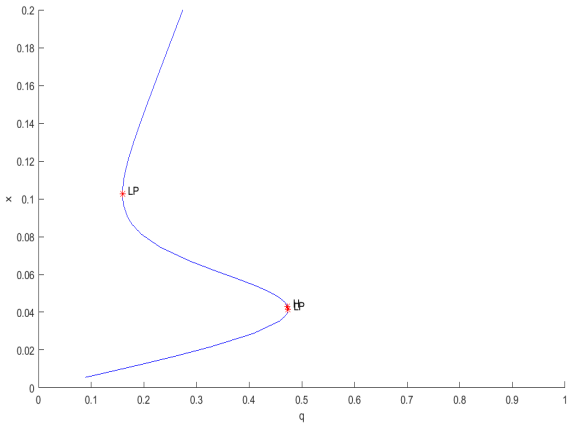

FIGURE 15. The bifurcation diagram for a wide range of the parameter q_*, $v_f = 15m/s$.

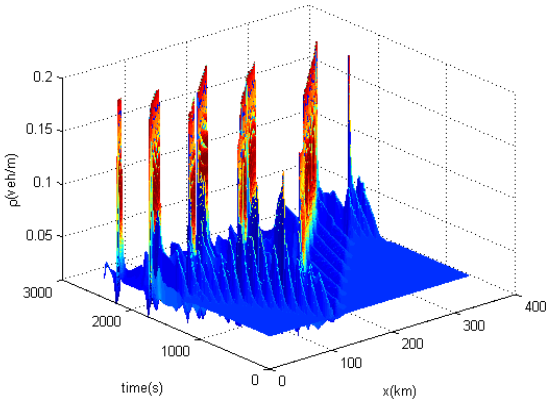

FIGURE 16. Density spatiotemporal graph with Hopf branch as initial value.

0.4723685. The state variables of it are $(0.041289, 0)$ and the corresponding vehicle density is $\rho_0 = 0.047889veh/m$. The characteristic values of it are $-5.15597e\,(-8) + i0.0163041$ and $-5.15597e\,(-8) - i0.0163041$. That is, the real parts of the pair of conjugate eigenvalues are 0. This is considered a mark of a Hopf bifurcation.

By substituting the value of ρ_0 into the Eq. $-(1-\rho_m\rho_0)^2 V_e'(\rho_0)$, we have $-(1-\rho_m\rho_0)^2 V_e'(\rho_0) = 1.6245$. Obviously, the inequality $1.6245 > 0.4723685 > 0$ satisfies the model's Hopf bifurcation existence conditions deduced in the section 4.1. The numerical results also confirm the theory obtained.

The first limit point bifurcation is appeared when the variable parameter q_* is taken as 0.48027. The state variables of it are $(0.040925, 0)$ and the corresponding vehicle density is $\rho_0 = 0.48054veh/m$. The characteristic values of it are -0.123508 and $8.18099\text{e} - 11$. That is, the second characteristic value is 0 and it is a mark of a limit point bifurcation. Moreover, the real part of the first characteristic value is negative. That means it is a stable limit point, namely a saddle-node bifurcation.

By substituting the value of ρ_0 into the Eq. $-(1-\rho_m\rho_0)^2 V_e'(\rho_0)$, we have $-(1-\rho_m\rho_0)^2 V_e'(\rho_0) = 0.1401$. Obviously, the equation $q_{*_0} = -(1-\rho_m\rho_0)^2 V_e'(\rho_0)$ satisfies the model's saddle-node bifurcation existence conditions deduced in the section 4.3. The numerical result is compatible with the analysis of theory.

The second limit point bifurcation is appeared when the variable parameter q_* is taken as 0.187918. The state variables of it are $(0.113602, 0)$ and the corresponding vehicle density is $\rho_0 = 0.1806veh/m$. The characteristic values of it are $3.69898e - 9$ and 0.0296604. That is, the first characteristic value is 0 and it is a mark of a limit point bifurcation.

By substituting the value of ρ_0 into the Eq. $-(1-\rho_m\rho_0)^2 V_e'(\rho_0)$, we have $-(1-\rho_m\rho_0)^2 V_e'(\rho_0) = 0.8872$. Obviously, the equation $q_{*_0} = -(1-\rho_m\rho_0)^2 V_e'(\rho_0)$ satisfies the model's saddle-node bifurcation existence conditions deduced in the section 4.3. The numerical result is compatible with the analysis of theory.

We still choose the above equilibrium point $(\rho_2, 0) = (0.0546, 0)$, and analyze the effect of the Hopf bifurcation in the time evolution of traffic density when $q_* = 0.2$ and $v_f = 15$m/s. By choosing the Hopf bifurcation point as the initial average density of the density time evolution, it may help to improve our understanding of complex phenomena in congested traffic. The traffic flow model analyzes the local disturbance under the initial uniform condition. Selecting the same numerical simulation conditions as above, at this time we choose $\rho_0 = 0.047889veh/m$ corresponding to the Hopf bifurcation point as the initial average density, and the time evolution of the density is shown in Figure 16.

It can be seen from Figure 16 that when the initial density value is within the unstable range of the model, as time increases, the amplitude of the initial small disturbance increases sharply in the early stage, the density fluctuation is very strongly, the cycle oscillation amplitude becomes very short. Finally, a strong and large-scale periodic oscillation is formed. The traffic flow is in an unstable state. This is a very obvious contrast between Figure 8 and Figure 13.

As the vehicle speed continues to decrease, the traffic density value gradually increases, the number of vehicles on the road section increases, the distance between vehicles becomes smaller, and the transportation system becomes unstable. Combining the density space-time diagram and the branch diagram at this time, it can be seen that when the variable parameter q_* passes through the Hopf branch point in the system, the transportation system still produces a periodic solution from the equilibrium point. The small disturbance of the initial uniform density is amplified and then evolved into a strong constant amplitude periodic oscillation. Small disturbances will change into stronger waves while walking and stopping. It further shows that the obtained results are consistent with actual phenomena and numerical simulation results.

We still choose the above equilibrium point $(\rho_2, 0) = (0.0546, 0)$, and analyze the effect of the LP bifurcation in the time evolution of traffic density when $q_* = 0.2$ and $v_f = 15$m/s. By choosing the LP bifurcation point as the initial average density of the density time evolution, it may help to improve our understanding of complex phenomena in

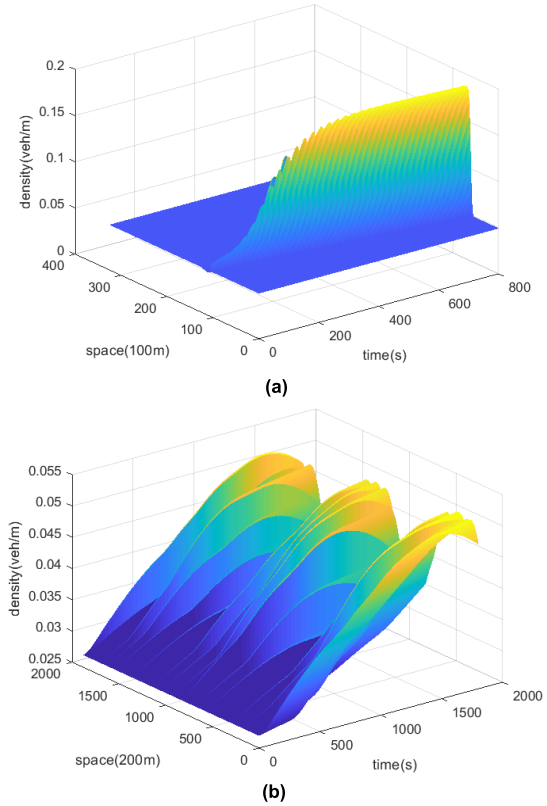

FIGURE 17. Density spatiotemporal graph with LP branch as initial value: (a) Phase plane diagram when the initial density $\rho_0 < 0.48054$veh/m; (b) Phase plane diagram when the initial density $\rho_0 > 0.48054$veh/m.

congested traffic. The traffic flow model analyzes the local disturbance under the initial uniform condition. Selecting the same numerical simulation conditions as above, at this time we choose $\rho_0 = 0.48054$ corresponding to the LP bifurcation point as the initial average density, and the time evolution of the density is shown in Figure 17.

From the above-mentioned density space-time graph, we can see that the vehicle speed drops to the lowest driving speed, the traffic volume increases sharply, the distance between vehicles changes to small, and the traffic system is congested sharply. The traffic system starts from the equilibrium point and will produce local clustering. The transportation system will generate local clusters from equilibrium points. Compared with Figure 14(a), as time increases, small disturbances are greatly amplified, and finally, high-density convergence is formed, and the traffic system is densely congested, as shown in Figure 17(a). It can be seen from Figure 17(b) that the small disturbance of the initial uniform density is greatly amplified and then evolved into a strong local aggregation phenomenon, that is, severe traffic congestion, which has a significant change from Figure 14(b). Compared with Figure 11 and Figure 14, the density spatio-temporal diagram at this time has obvious changes.

From $v_f = 30$m/s to $v_f = 15$m/s, the corresponding branch diagram and density space-time diagram can be seen that with the increase of time, the density of vehicle flow increases, the speed of vehicles decreases, the distance between vehicles becomes smaller, and the traffic congestion intensify. When $v_f = 30$m/s, the speed is taken as a constant speed, the density space-time graph drawn with the Hopf branch point can see the phenomenon of constant amplitude oscillation. With the increase of traffic volume and the decrease of vehicle speed, when $v_f = 20$m/s, the density spatiotemporal map drawn with Hopf branch points reflects that the frequency of constant amplitude oscillation is more, and the interval of constant amplitude oscillation becomes smaller, which indicates that congestion happened earlier, and the phenomenon of stopping while walking has continued. When $v_f = 15$m/s, the traffic flow speed is already in a low state. It can be seen that when the density space-time map was drawn by the Hopf branch point is 0-100km, the constant amplitude oscillation has already occurred, and the tidal oscillation has formed, which shows that, at this time, the traffic system quickly reached a state of congestion and reached a climax. At the same time, when $v_f = 30$m/s, the density space-time map was drawn with saddle-node branch points can see the sudden change of traffic stability and the occurrence of local clustering. With the increase of traffic volume and the decrease of vehicle speed, when $v_f = 20$m/s, the density space-time map was drawn with the saddle-node branch point reflects the change process of the traffic system from a stable state to a congested state. When the parameter changes and exceeds the critical value, the qualitative state of the system such as free-running state, blocking state, stop-and-go, etc. will change suddenly. When $v_f = 15$m/s, it can be seen that the average density value of the road section in the density space-time graph was drawn by the saddle-node branch point gradually increases with time fluctuations, indicating that the disturbance in the traffic flow is amplified and the traffic system tends to be unstable. This is consistent with the actual traffic flow, which further verifies the correctness of the theoretical results.

VI. CONCLUSION

To describe and predict the nonlinear traffic phenomenon of the urban road from the perspective of global stability, this paper changes the traveling wave of the macro traffic flow model based on the speed difference of different driving characteristics, thus obtaining a new model suitable for traffic flow stability analysis. At the same time, the branch analysis of the macro traffic flow model is conducted. The article first discusses the types of system equilibrium points and their stable states. Secondly, for further analysis and comparison, the researcher chooses four sets of parameters to describe the global distribution structure of the trajectory on the phase plane diagram, and the data results show that this method is consistent with the theoretical analysis. After that, the conditions of Hopf bifurcation and saddle-node bifurcation are derived, and the types of Hopf bifurcation are discussed further. Taking the balance point in the model as an example, we can obtain various system branches, such as

Hopf branch, saddle-node branch, limit cycle branch, cusp branch, BT branch by choosing different parameters as the continuous variable parameters of the system, which indicates that the theoretical and numerical results can be verified with each other. Starting from the Hopf branch and the saddle knot branch, the stop-and-walk phenomenon and the stability mutation phenomenon of urban roads can be better explained by drawing the phase plane diagram and density space-time diagram of the system. The experimental results show that the branch analysis method can provide a detailed theoretical basis for the implementation of traffic control strategies.

CONFLICT OF INTERESTS

The authors declare that there is no conflict of interests regarding the publication of this paper.

ACKNOWLEDGMENT

The authors would like to thank the anonymous referees and the editor for their valuable opinions.

REFERENCES

[1] G. Zhang, Y. Zhang, D.-B. Pan, and C.-Y. Sang, "Study on the interval integration effect of vehicle's self-delayed velocity on traffic stability in micro traffic modeling," *Phys. A, Stat. Mech. Appl.*, vol. 533, Nov. 2019, Art. no. 121941.

[2] B.-G. Cao, "A car-following dynamic model with headway memory and evolution trend," *Phys. A, Stat. Mech. Appl.*, vol. 539, Feb. 2020, Art. no. 122903.

[3] W. Shi, Y.-F. Wei, T. Song, S.-Q. Dai, and L.-Y. Dong, "Anticipation driving behavior and related reduction of energy consumption in traffic flow," *Int. J. Mod. Phys. C*, vol. 21, no. 7, pp. 915–929, Jul. 2010.

[4] T. Wang, J. Zhao, and P. Li, "An extended car-following model at un-signalized intersections under V2V communication environment," *PLoS ONE*, vol. 13, no. 2, Feb. 2018, Art. no. e0192787.

[5] G. O. Fosu, F. T. Oduro, and C. Caligaris, "Multilane analysis of a viscous second-order macroscopic traffic flow model," *Social Netw. Partial Differ. Equ. Appl.*, vol. 2, no. 1, pp. 1–17, Feb. 2021.

[6] N. Laurent-Brouty, A. Keimer, P. Goatin, and A. M. Bayen, "A macroscopic traffic flow model with finite buffers on networks: Well-posedness by means of Hamilton–Jacobi equations," *Commun. Math. Sci.*, vol. 18, no. 6, pp. 1569–1604, 2020.

[7] P. Zhang, Y. Xue, Y.-C. Zhang, X. Wang, and B.-L. Cen, "A macroscopic traffic flow model considering the velocity difference between adjacent vehicles on uphill and downhill slopes," *Mod. Phys. Lett. B*, vol. 34, no. 21, Jul. 2020, Art. no. 2050217.

[8] M. Sreekumar, S. M. Joshi, A. Chatterjee, and T. V. Mathew, "Analyses and implications of higher order finite volume methods on first-order macroscopic traffic flow models," *Transp. Lett.*, vol. 11, no. 10, pp. 542–557, Nov. 2019.

[9] T. Hundesa, L. Lemecha, and P. R. Koya, "One-dimensional explicit Tolesa numerical scheme for solving first order hyperbolic equations and its application to macroscopic traffic flow model," *Appl. Math.*, vol. 10, no. 3, pp. 119–137, 2019.

[10] Y.-Q. Wang, X.-J. Chu, C.-F. Zhou, B.-W. Yan, B. Jia, and C.-H. Fang, "Wave dynamics in an extended macroscopic traffic flow model with periodic boundaries," *Mod. Phys. Lett. B*, vol. 32, no. 16, Jun. 2018, Art. no. 1850168.

[11] A. Iovine, F. Valentini, E. De Santis, M. D. Di Benedetto, and M. Pratesi, "Safe human-inspired mesoscopic hybrid automaton for autonomous vehicles," *Nonlinear Anal., Hybrid Syst.*, vol. 25, pp. 192–210, Aug. 2017.

[12] R. D. Pace, G. E. Cantarella, S. de Luca, and M. D. Gangi, "Scheduled synchronisation based on a mesoscopic flow model with speed dispersion," *Transp. Res.*, vol. 27, pp. 180–187, Jan. 2017.

[13] Y. Kim, S. Choi, J. Park, and H. Yeo, "Agent-based mesoscopic urban traffic simulation based on multi-lane cell transmission model," *Proc. Comput. Sci.*, vol. 151, pp. 240–247, Jan. 2019.

[14] Y. Igarashi, K. Itoh, K. Nakanishi, K. Ogura, and K. Yokokawa, "Bifurcation phenomena in the optimal velocity model for traffic flow," *Phys. Rev. E, Stat. Phys. Plasmas Fluids Relat. Interdiscip. Top.*, vol. 64, no. 4, Sep. 2001, Art. no. 047102.

[15] L. A. Safonov, E. Tomer, V. V. Strygin, Y. Ashkenazy, and S. Havlin, "Multifractal chaotic attractors in a system of delay-differential equations modeling road traffic," *Chaos, Interdiscipl. J. Nonlinear Sci.*, vol. 12, no. 4, pp. 1006–1014, Dec. 2002.

[16] H. J. C. Huijberts, "Analysis of a continuous car-following model for a bus route: Existence, stability and bifurcations of synchronous motions," *Phys. A, Stat. Mech. Appl.*, vol. 308, nos. 1–4, pp. 489–517, May 2002.

[17] G. Orosz, R. E. Wilson, and B. Krauskopf, "Global bifurcation investigation of an optimal velocity traffic model with driver reaction time," *Phys. Rev. E, Stat. Phys. Plasmas Fluids Relat. Interdiscip. Top.*, vol. 70, no. 2, Aug. 2004, Art. no. 026207.

[18] I. Gasser, G. Sirito, and B. Werner, "Bifurcation analysis of a class of 'car following' traffic models," *Phys. D, Nonlinear Phenomena*, vol. 197, nos. 3–4, pp. 222–241, Oct. 2004.

[19] L. Lijun, W. Chunyu, and H. Guoguang, "A review of bifurcation phenomena in traffic flow models," *Syst. Eng.*, no. 8, pp. 23–26, 2006.

[20] Z. Wei, L. Zhimin, C. Yandong, and Y. Jianning, "Period-doubling bifurcation and chaos in a new type of traffic flow car-following model," *J. Gansu Sci.*, vol. 20, no. 4, pp. 143–146, 2008.

[21] L. Daijian and X. Peng, "Stability and bifurcation characteristics of a class of nonlinear car-following models," *J. Traffic Transp. Eng. Inf.*, vol. 7, no. 4, pp. 6–11, 2009.

[22] J. Yan-Fei and X. Meng, "Bifurcation analysis of the full velocity difference model," *Chin. Phys. Lett.*, vol. 27, no. 4, Apr. 2010, Art. no. 040501.

[23] X. Jian and X. Ronggai, "Time-delayed car-following model and its bifurcation phenomenon," *Adv. Mech.*, vol. 43, no. 1, pp. 29–38, 2013.

[24] J. Delgado and P. Saavedra, "Global bifurcation diagram for the Kerner–Konhäuser traffic flow model," *Int. J. Bifurcation Chaos*, vol. 25, no. 5, May 2015, Art. no. 1550064.

[25] Y. Miura and Y. Sugiyama, "Coarse analysis of collective behaviors: Bifurcation analysis of the optimal velocity model for traffic jam formation," *Phys. Lett. A*, vol. 381, no. 48, pp. 3983–3988, Dec. 2017.

[26] Y.-Q. Wang, B.-W. Yan, C.-F. Zhou, W.-K. Li, and B. Jia, "Bifurcation analysis of a heterogeneous traffic flow model," *Mod. Phys. Lett. B*, vol. 32, no. 9, Mar. 2018, Art. no. 1850118.

[27] W. Wei, Z. Yong, and Z. Bing, "Stability and bifurcation analysis of low-dimensional macroscopic traffic flow model," *Math. Pract. Knowl.*, vol. 48, no. 7, pp. 230–237, 2018.

[28] W. Ren, R. Cheng, and H. Ge, "Bifurcation analysis of a heterogeneous continuum traffic flow model," *Appl. Math. Model.*, vol. 94, pp. 369–387, Jun. 2021.

[29] S. Zhu, Y. Zhao, Y. Zhang, Q. Li, W. Wang, and S. Yang, "Short-term traffic flow prediction with wavelet and multi-dimensional Taylor network model," *IEEE Trans. Intell. Transp. Syst.*, vol. 22, no. 5, pp. 3203–3208, May 2021.

[30] A. Miglani and N. Kumar, "Deep learning models for traffic flow prediction in autonomous vehicles: A review, solutions, and challenges," *Veh. Commun.*, vol. 20, Dec. 2019, Art. no. 100184.

[31] X. Chen, L. Li, and Q. Shi, "Stochastic evolutions of dynamic traffic flow," in *Modeling and Applications*. Berlin, Germany: Springer, 2015.

[32] D. Ngoduy and T. Li, "Hopf bifurcation structure of a generic car-following model with multiple time delays," *Transportmetrica A, Transp. Sci.*, vol. 17, no. 4, pp. 878–896, Dec. 2021.

[33] D. Ngoduy, S. Lee, M. Treiber, M. Keyvan-Ekbatani, and H. L. Vu, "Langevin method for a continuous stochastic car-following model and its stability conditions," *Transp. Res. C, Emerg. Technol.*, vol. 105, pp. 599–610, Aug. 2019.

[34] D. Jia and D. Ngoduy, "Enhanced cooperative car-following traffic model with the combination of V2V and V2I communication," *Transp. Res. B, Methodol.*, vol. 90, pp. 172–191, Aug. 2016.

[35] S. P. Hoogendoorn and P. H. L. Bovy, "Continuum modeling of multiclass traffic flow," *Transp. Res. B, Methodol.*, vol. 34, no. 2, pp. 123–146, Feb. 2000.

[36] J. F. Cao, C. Z. Han, and Y. W. Fang, *Nonlinear Systems Theory and Application*, Xi'an, China: Xi'an Jiao Tong Univ. Press, 2006.

[37] W.-H. Ai, Z.-K. Shi, and D.-W. Liu, "Bifurcation analysis of a speed gradient continuum traffic flow model," *Phys. A, Stat. Mech. Appl.*, vol. 437, pp. 418–429, Nov. 2015.

[38] W. Ai, Z. Shi, and D. Liu, "Bifurcation analysis method of nonlinear traffic phenomena," *Int. J. Mod. Phys. C*, vol. 26, no. 10, Oct. 2015, Art. no. 1550111.